

Two of a Kind: Comparing big and small black holes in binaries with gravitational wavesAMANDA M. FARAH ¹, MAYA FISHBACH ² AND DANIEL E. HOLZ ^{1,3,4}¹*Department of Physics, University of Chicago, Chicago, IL 60637, USA*²*Canadian Institute for Theoretical Astrophysics, David A. Dunlap Department of Astronomy and Astrophysics, and Department of Physics, 60 St George St, University of Toronto, Toronto, ON M5S 3H8, Canada*³*Kavli Institute for Cosmological Physics, The University of Chicago, 5640 South Ellis Avenue, Chicago, Illinois 60637, USA*⁴*Enrico Fermi Institute, The University of Chicago, 933 East 56th Street, Chicago, Illinois 60637, USA*

ABSTRACT

When modeling the population of merging binary black holes, analyses generally focus on characterizing the distribution of primary (i.e. more massive) black holes in the binary, while simplistic prescriptions are used for the distribution of secondary masses. However, the secondary mass distribution provides a fundamental observational constraint on the formation history of coalescing binary black holes. If both black holes experience similar stellar evolutionary processes prior to collapse, as might be expected in dynamical formation channels, the primary and secondary mass distributions would show similar features. If they follow distinct evolutionary pathways (for example, due to binary interactions that break symmetry between the initially more massive and less massive star), their mass distributions may differ. We explicitly fit the secondary mass distribution, finding that if the primary and secondary mass distributions are different, the previously-identified peak in the primary mass distribution may be driven by an even larger peak in the secondary mass distribution. Alternatively, if we assume that the two masses are drawn from the same underlying distribution, they both show a peak at $31.4_{-2.6}^{+2.3} M_{\odot}$. This value is shifted lower than that obtained when assuming the peak only exists in the marginal primary mass distribution, placing this feature in further tension with expectations from a pulsational pair-instability supernova pileup. We anticipate that by the end of the fifth LIGO-Virgo-KAGRA observing run, we will be able to determine whether the data prefer distinct or identical component mass distributions to $> 4\sigma$, providing important clues to the formation history of coalescing binary black holes.

Keywords: Gravitational waves(678) — Binary stars(154) — Compact objects(288) — Astronomy data analysis(1858)

1. INTRODUCTION

Dozens of gravitational-wave (GW) events have been observed by the LIGO (Aasi et al. 2015), Virgo (Acernese et al. 2014) and KAGRA (Akutsu et al. 2021) detector network (Abbott et al. 2021a), and many more detections are anticipated by the end of the fourth observing run. However, the formation mechanism of binary black hole (BBH) mergers, which source the majority of the detected GW events, is still largely uncertain. While it is not possible to know the formation history of any one BBH with certainty, the population of all

merging BBHs is thought to encode information about which astrophysical processes give rise to the bulk of these systems (e.g. Stevenson et al. 2015; Zevin et al. 2017).

The stellar-mass BBHs detectable by LIGO, Virgo and KAGRA are likely created from the collapse of massive stars. These massive stars may be born as a binary system in the galactic field that then evolves into a BBH system. Alternatively, they may be born in a dense stellar environment, such as a star cluster, in which the BH stellar remnants dynamically assemble into tightly-bound binaries. The population of GW sources therefore contains signatures of the initial conditions of their progenitor stellar systems, as well as many of the evolutionary processes that occur between star formation

and BBH merger. The initial conditions that impact the GW source population include the initial mass function of either binary or single stars (binary IMF and IMF, respectively) in different environments, the birth metallicities, and other aspects of their formation environments. Depending on the dominant formation scenario of BBHs, the evolutionary processes that are imprinted in the BBH population include stellar mass loss, transfer of matter between two component stars, the supernova process for massive stars, and dynamical interactions in star clusters or the disks of active galactic nuclei (see reviews by [Mapelli 2020](#); [Mandel & Farmer 2022](#), and references therein).

In general, these uncertain formation processes affect the masses, spins, redshifts, and merger rates of BBH systems. Here we focus on the BBH mass distribution, since BH masses are well-measured from the GW signal. The BBH mass distribution is typically parameterized by the primary mass m_1 , the larger of the two component masses in the binary, and either the secondary mass m_2 , or the mass ratio $q = m_2/m_1$. Within these parametrizations, it is typically assumed either that the primary and secondary masses follow the same underlying distribution ([Fishbach & Holz 2020](#); [Doctor et al. 2020](#); [Farah et al. 2022](#); [Edelman et al. 2022b](#); [Abbott et al. 2023a](#); [Sadiq et al. 2023](#)), or that the primary mass distribution has distinct features from the secondary mass distribution. The latter assumption implies that primary and secondary mass are physically meaningful labels and is typically achieved by modeling the secondary mass distribution as a single power law between some minimum mass and m_1 ([Fishbach & Holz 2017a](#); [Kovetz et al. 2017](#); [Talbot & Thrane 2018](#); [Baxter et al. 2021](#); [Abbott et al. 2021b](#); [Tiwari 2021](#); [Abbott et al. 2023a](#); [Edelman et al. 2022a](#); [Callister & Farr 2023](#); [Godfrey et al. 2023](#)). The former assumption—that m_1 and m_2 follow the same underlying distribution—implies that the two-dimensional mass distribution is symmetric in primary and secondary mass, meaning that m_1 and m_2 can be interchanged without changing the mass distribution. Neither of these assumptions have been explicitly verified with the available data. In this work, we aim to determine whether both components in merging BBHs follow the same underlying distribution, or whether there is a physical distinction between primary and secondary masses.

Understanding whether the primary and secondary masses in BBH mergers follow the same distribution will provide insight into their formation histories. For BBH mergers that are dynamically assembled in dense environments, we expect that both component BHs are drawn from the same population of stellar remnants (i.e.

m_1 and m_2 are arbitrary labels), and we expect the two-dimensional BBH mass distribution to be symmetric in m_1 and m_2 . On the other hand, for BBH mergers that originate from binary stars that formed and evolved in relative isolation (“field binaries”), there may be a physical distinction between primary and secondary BH component masses. To start off, the progenitor stars in the binary are drawn from the binary IMF, which may not be symmetric between the two components (e.g. [Grudić et al. 2023](#)). Furthermore, the two stars exchange mass during binary stellar evolution. In each phase of mass transfer, one component acts as the donor and the other as the accretor, depending on their initial masses. Mass transfer affects the stellar structure of the donor and the accretor in different ways, and can impact the masses of the resulting BHs following stellar collapse ([Laplace et al. 2021](#)).

In short, binary stellar evolution consists of several processes that can break the symmetry between the population of initially more massive stars, which generally correspond to the first born and more massive (primary) BHs and the population of initially less massive stars, which generally correspond to the second born and less massive (secondary) BHs. However, if mass inversion occurs in some systems, some initially less massive stars will end up as the more massive BH by the time of BBH merger, and the distribution of primary BH masses will have contributions from both the second-born and first-born BHs ([Olejak & Belczynski 2021](#); [Hu et al. 2022](#); [Broekgaarden et al. 2022](#); [Zevin & Bavera 2022](#)). If mass inversion happens in exactly half of merging BBH systems, the primary and secondary component mass distributions may be indistinguishable even if the first and second born distributions are distinct.

From a data analysis perspective, knowing that the primary and secondary mass distributions are the same allows us to measure a single set of model parameters: those of the shared distribution. This may allow features of the distribution to be measured with higher precision since both components in the binary will contribute to the measurement of each feature, rather than just the primary mass. Furthermore, disentangling the role of primary and secondary masses aids the physical interpretations of such features.

For example, [Abbott et al. \(2023a\)](#) found that the mass distribution exhibits a peak at primary masses $m_1 \sim 35 M_\odot$. The astrophysical origin of this over-density in the mass distribution is uncertain, although it may be related to (pulsational) pair-instability supernovae (e.g. [Heger & Woosley 2002](#); [Fishbach & Holz 2017b](#); [Talbot & Thrane 2018](#); [Farmer et al. 2019](#)). A necessary ingredient towards understanding the origin of

the $m_1 \sim 35 M_\odot$ peak is to first understand whether the peak appears exclusively among primary BBH masses, or whether secondary masses also display a peak, indicating that secondary BHs also experience the astrophysical process that leads to a mass pileup.

This paper is organized as follows. In Section 2 we describe the different population models considered in this work. In Section 3 we present the results of fitting each of the models to the Third Gravitational-Wave Transient Catalog (GWTC-3 [Abbott et al. 2021a](#)), finding that while the primary and secondary masses of merging BBHs are consistent with following the same underlying distribution, it is also possible that the secondary mass distribution has a more prominent peak than does the primary mass distribution. In Section 4 we discuss possibilities for future observations. In Section 5 we summarize our conclusions and present possible astrophysical interpretations of our results. The appendices discuss the fundamental differences between commonly-used parametrizations for the two-dimensional mass distribution and include details about the population models and statistical framework.

2. POPULATION MODELS

Because our aim is to learn whether the primary and secondary masses are consistent with being drawn from the same distribution, we describe the primary and secondary mass distributions separately, but according to the same functional form. We model each of the one-dimensional mass distributions as a mixture model between a smoothed power law component and a Gaussian component G in order to make direct comparisons to the POWER LAW + PEAK model used by the LIGO-Virgo-KAGRA’s (LVK) population analysis to describe the distribution of primary masses ([Talbot & Thrane 2018](#); [Abbott et al. 2021b, 2023a](#)).

There are several ways to construct a two-dimensional mass model for the binary from this one-dimensional mass model for the component masses. However, as we discuss in Appendix A, in order to explicitly compare primary and secondary mass distributions, it is necessary to use the pairing function framework first introduced for GW population modeling in [Fishbach & Holz \(2020\)](#). Explicitly,

$$p(m_1, m_2 | \Lambda) = p_1(m_1 | \Lambda_1) p_2(m_2 | \Lambda_2) f(q; \beta_q), \quad (1)$$

where $p_1(m_1 | \Lambda_1)$ is the underlying distribution of primary masses, $p_2(m_2 | \Lambda_2)$ is the underlying distribution of secondary masses, $f(q)$ is a pairing function that de-

pends on the mass ratio of the system¹, Λ_1 and Λ_2 are the hyperparameters² describing the underlying primary and secondary mass distributions, respectively, and $\Lambda = \{\Lambda_1, \Lambda_2, \beta_q\}$ is the set of all mass model hyperparameters. In this work, we use a pairing function of the form $f(q; \beta_q) = q^{\beta_q} \Theta(q \leq 1)$, though other forms may provide a better fit to the data (e.g. [Farah et al. 2022](#)).

As illustrated in Figure 1, different choices for the relationship between Λ_1 and Λ_2 result in distinct morphologies for the two-dimensional mass distribution. Below, we list each of the variations we consider in this work, along with the panels in Figure 1 to which they correspond. A table describing these variations in terms of choices for the hyper-prior is given in Appendix B.3.

- **PAIRING:SYMMETRIC:** This model sets $\Lambda_1 = \Lambda_2$, making the distribution symmetric under the transformation $m_1 \leftrightarrow m_2$. It corresponds to the first row of Figure 1: any feature in one of the distributions has to be present in both, so it always makes two bands that connect on the diagonal.
- **PAIRING:GENERIC:** This model allows the hyperparameters describing the $\sim 35 M_\odot$ peak to differ between $p_1(m_1 | \Lambda_1)$ and $p_2(m_2 | \Lambda_2)$. It can produce any of the panels in Figure 1, and is the only model that can produce a scenario such as that illustrated in the middle panel, where the feature in one direction is more prominent and in a different location than the feature in another direction.
- **PAIRING:NO PEAK IN $p_2(m_2)$:** This model sets all $\Lambda_2 = \Lambda_1$, except for the parameter governing the height of the $\sim 35 M_\odot$ peak, which we set to vanish for the secondary mass distribution but we fit as a free parameter for the primary mass distribution. This model corresponds to the bottom row of Figure 1: it is only capable of having a peak in the primary mass distribution, so can only produce vertical bands in a two-dimensional mass distribution. In Appendix A.3, we show that PAIRING:NO PEAK IN $p_2(m_2)$ approximately mimics the behavior of the commonly-used POWER LAW + PEAK model from, e.g., [Abbott et al. \(2023a\)](#), which we refer to as LVK 2023.

¹ In principle, the pairing function can be parameterized in terms of any observable parameter (e.g., total mass).

² We use the term “hyperparameter” for a model parameter that describes the population of merging compact binaries, in contrast to the parameters describing each individual GW detection, such as a system’s masses and spins.

The different columns in Figure 1 correspond to different power law spectral indices, β_q , for the mass ratio-dependent pairing function. The leftmost panels show models where components in the binary are allowed to pair up independently of mass ratio, the middle column shows a model where components have a slight preference to pair up with partners that are equal mass, and the rightmost panel shows the case where components are very “picky”: they almost always pair up with equal mass partners (Fishbach & Holz 2020). When components pair near-independently of mass ratio, the asymmetric models produce noticeably different distributions than the symmetric models. However, in the case of very picky binaries, the two scenarios become difficult to tell apart. There is therefore a degeneracy between the steepness of the pairing function and the existence of distinct features in the two mass distributions (see Tiwari 2023, for a discussion of this phenomenon in terms of Jacobian transformations).

In all models considered in this work, the redshift distribution is modeled as a power law with spectral index κ (Fishbach et al. 2018). We use the DEFAULT spin model from Abbott et al. (2021b, 2023a) to describe the spin magnitudes and tilts of each component. These are the same redshift and spin distributions used with the POWER LAW + PEAK mass model in the analysis presented in Abbott et al. (2023a). The explicit form of the full population model is given in Appendix B.

Using these parameterized models, we construct a hierarchical Bayesian inference (described in Appendix C) to determine the appropriate population-level parameters for the mass distribution, Λ , given the observed set of data $\{D_j\}$ for N observed events (Loredo 2004; Mandel et al. 2019). We model the data as an inhomogeneous Poisson process with the rate density (number of events per unit time per single-event-parameter hypervolume) given by

$$\frac{d\mathcal{N}}{dm_1 dm_2, ds_1 ds_2 dz} = \mathcal{R} p(z) p(s_1, s_2) p(m_1, m_2 | \Lambda), \quad (2)$$

where \mathcal{R} acts as a normalizing constant that sets the overall magnitude of the rate.

3. RESULTS

We fit each model described in Section 2 to the BBHs in GWTC-3. The resulting average two-dimensional posterior population distribution (PPD) for the PAIRING:SYMMETRIC and PAIRING:GENERIC models are shown in Figure 2. The contours differ in morphology to those illustrated in Figure 1 because the actual distribution of BBH component masses exhibits two peaks: one at $\sim 10 M_\odot$ and another at $\sim 35 M_\odot$ (Abbott et al. 2021b; Tiwari 2021; Edelman et al. 2022a;

Sadiq et al. 2022; Abbott et al. 2023a; Edelman et al. 2022b; Farah et al. 2023; Ray et al. 2023), whereas we only place one peak in the models shown in Figure 1. The peak at $\sim 10 M_\odot$ creates bands in all panels that have very little vertical extent because the peak is proximal to the minimum BH mass. Nonetheless, fits using both models exhibit vertical and horizontal bands, indicating peaks in both $p_1(m_1)$ and $p_2(m_2)$. While the PAIRING:SYMMETRIC model requires this behavior, the PAIRING:GENERIC model does not, meaning that the secondary mass distribution appears to exhibit its own feature at $\sim 35 M_\odot$. Furthermore, the fact that PAIRING:GENERIC produces a PPD similar to that of PAIRING:SYMMETRIC indicates that the data support consistent primary and secondary mass distributions.

The bands in all panels do not go the full extent of parameter space but rather taper off away from the diagonal, indicating a preference for equal-mass binaries either through a pairing function or a mass ratio distribution that favors $m_1 \approx m_2$.

3.1. Primary and secondary masses are consistent with having the same underlying distribution

The underlying distributions (i.e. before a pairing function is applied) of the primary and secondary masses are shown in Figure 3 for the two pairing function models. There is a region of overlap between the primary and secondary mass distributions under the PAIRING:GENERIC model, indicating that the primary and secondary mass distributions are consistent with one another. As expected, this region of overlap also coincides with $p(m)$, the distribution describing both component masses in the PAIRING:SYMMETRIC model.

Models not explicitly parameterized in terms of a pairing function are unable to produce underlying distributions such as those shown in Figure 3, so for the sake of comparison to previous work, we turn to conditional³ m_2 distributions, $p(m_2 | m_1 = C)$, where C can be any number in the domain of the m_1 distribution. Figure 4 shows these conditional distributions for the PAIRING:SYMMETRIC, PAIRING:GENERIC and POWER LAW + PEAK model presented in Abbott et al. (2023a) (herein LVK 2023), which does not use a pairing function. The curves in Figure 4 represent an average over the hyper-posterior for each model; this average is sometimes referred to as a posterior population distribution (PPD).

³ While marginal distributions are typically used for the purpose of comparing PPDs from several models on a single plot, they are not sensitive to differences between two-dimensional mass distributions when equal masses are preferred (see Appendix B.3), so we use conditional distributions instead.

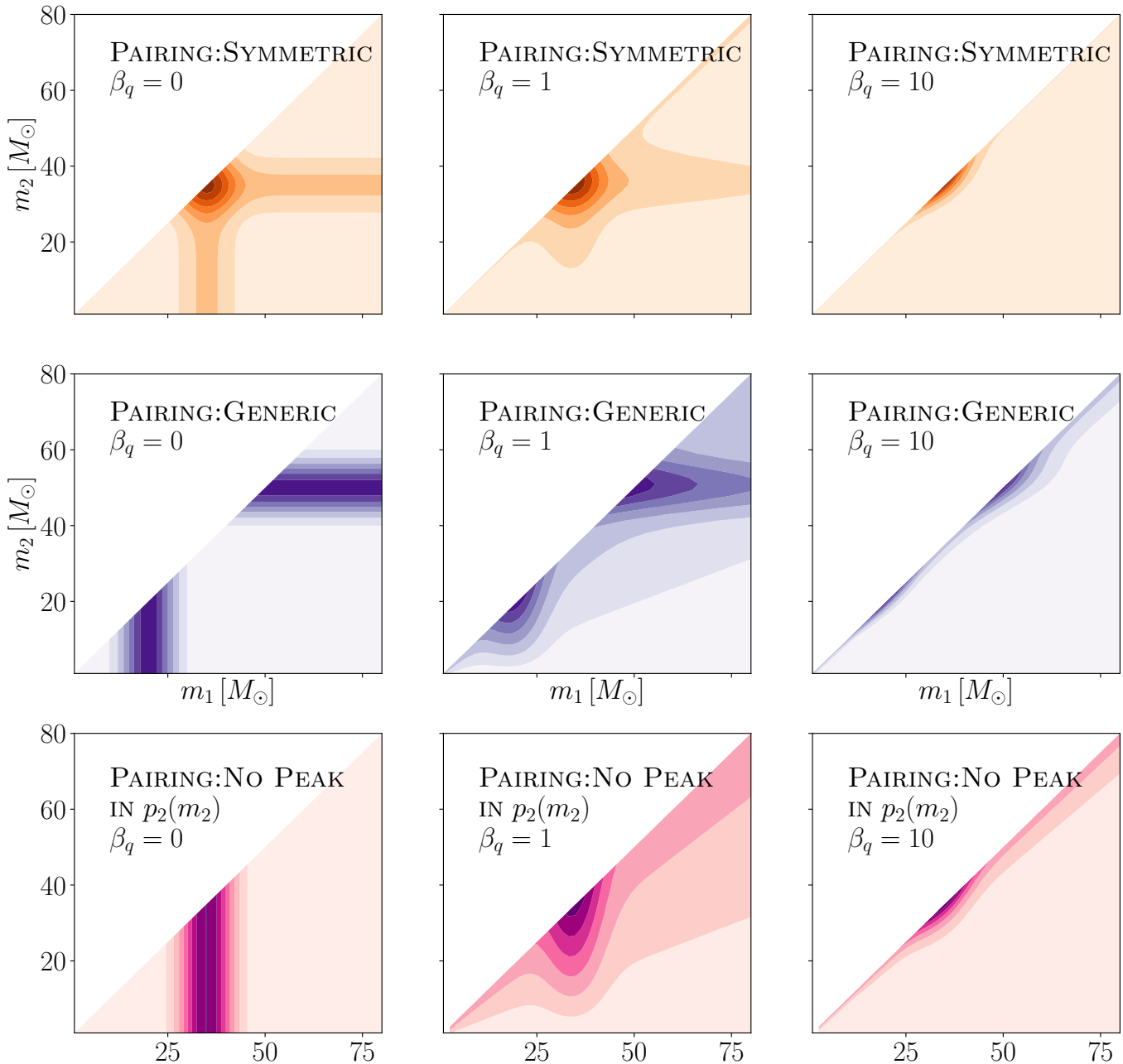


Figure 1. Illustration of some possible two-dimensional mass distributions under the models considered in this work. Overdensities/peaks in the mass distribution appear as darker filled contours in these figures. The different columns correspond to different power law spectral indices for the mass ratio-dependent pairing function, β_q . In the case where components strongly prefer to pair with nearly equal-mass partners, it becomes difficult to determine whether a feature appears only in one component mass distribution (as in the PAIRING:NO PEAK IN $p_2(m_2)$ model, *bottom row*) or in both (PAIRING:SYMMETRIC, *top row*) become difficult to tell apart and likely explain the data equally well. The diagonal contours in the middle and right columns are caused by a preference for equal-mass binaries and follow lines of constant mass ratio. The goal of this paper is to distinguish between the different scenarios illustrated in this figure.

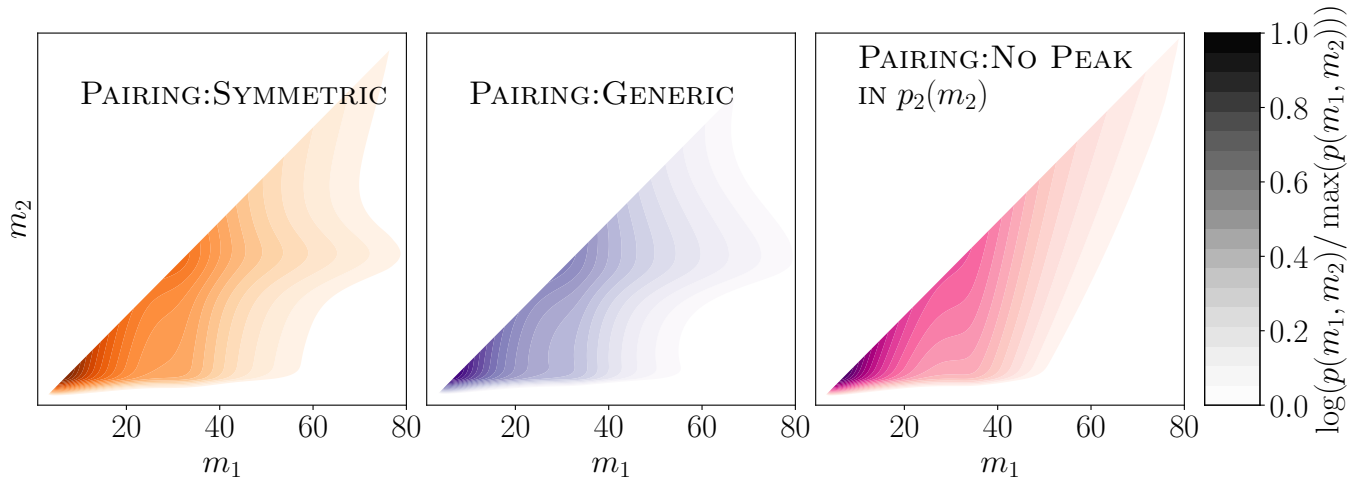


Figure 2. Two-dimensional posterior population distributions (PPDs) for PAIRING:SYMMETRIC (*left, orange*), PAIRING:GENERIC (*middle, purple*), and PAIRING:NO PEAK IN $p_2(m_2)$ (*right, pink*), all fit to the BBHs in GWTC-3. Darker colors indicate a higher rate of sources, and each panel is individually normalized to its maximum value. All three models find a higher rate of events near the $m_1 = m_2$ diagonal, as well as peaks at $m_1 \sim 10 M_\odot$ and $m_1 \sim 35 M_\odot$, which appear as vertical bands in all three panels. PAIRING:SYMMETRIC and PAIRING:GENERIC both find peaks in m_2 as well, as indicated by horizontal bands in the two rightmost panels, whereas PAIRING:NO PEAK IN $p_2(m_2)$ is unable to model features in the m_2 direction. Additionally, PAIRING:SYMMETRIC and PAIRING:GENERIC display peaks in similar locations despite the fact that PAIRING:SYMMETRIC requires that both m_1 and m_2 follow the same underlying distribution while PAIRING:GENERIC is able to model each component separately. This suggests that both components are drawn from the same underlying distribution, up to a pairing function.

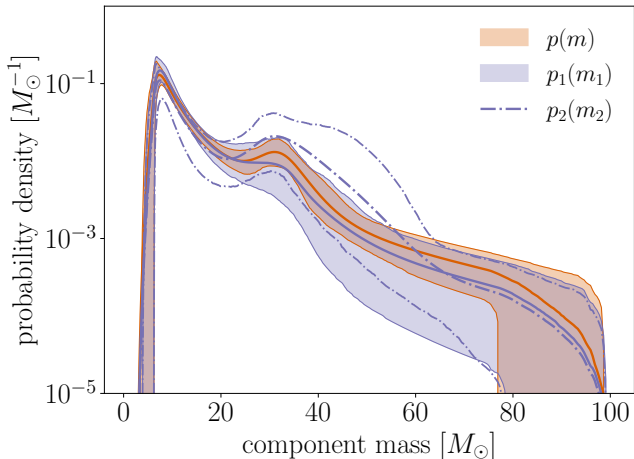


Figure 3. Underlying distribution of primary and secondary masses for the PAIRING:SYMMETRIC (orange) and PAIRING:GENERIC (purple) models. Under the PAIRING:SYMMETRIC model, $p_1(m_1) = p_2(m_2) \equiv p(m)$, so only $p(m)$ is shown. $p(m)$ under PAIRING:SYMMETRIC is more tightly constrained than $p_1(m_1)$ (purple filled band) or $p_2(m_2)$ (dot-dashed lines) under PAIRING:GENERIC as it has twice as many observations per free parameter. These distributions are constructed to describe the population of black holes *before* the function that pairs components into merging binaries is applied. All three underlying distributions are consistent with one another, though $p_2(m_2)$ appears to have a large peak at $\sim 35 M_\odot$ while $p_1(m_1)$ has some support for no peak in that region. $p(m)$ does not have support for no peak, but its peak is constrained to be small, while the peak in $p_2(m_2)$ is less well-constrained and may be larger in amplitude. This hints at the possibility that the peak identified in the primary mass distribution by the LVK 2023 formalism may have been driven by a peak in $p_2(m_2)$ rather than $p_1(m_1)$, though hyperparameter uncertainties within PAIRING:GENERIC are too large to definitively determine this, and the data is consistent with $p_1(m_1) = p_2(m_2)$.

For all values of C , the inferred distribution under the PAIRING:GENERIC model behaves similarly to that of the PAIRING:SYMMETRIC model, indicating consistency between the primary and secondary mass distributions. In particular, under the PAIRING:SYMMETRIC and PAIRING:GENERIC models, we see a peak in the conditional secondary mass distribution $p(m_2|m_1 = C)$ when $C \geq 35 M_\odot$ (solid and dotted lines). While m_2 generally prefers to be near m_1 , as indicated by an upward trend in all models, the two pairing function models have more support for m_2 being within the peak than being nearly equal to m_1 when m_1 is large (dotted lines). This behavior is in contrast to the LVK 2023 model, which forces the conditional secondary mass distribution $p(m_2|m_1 = C)$ to monotonically increase for all values of C because it does not allow for a peak in m_2 . While the PAIRING:GENERIC model can replicate

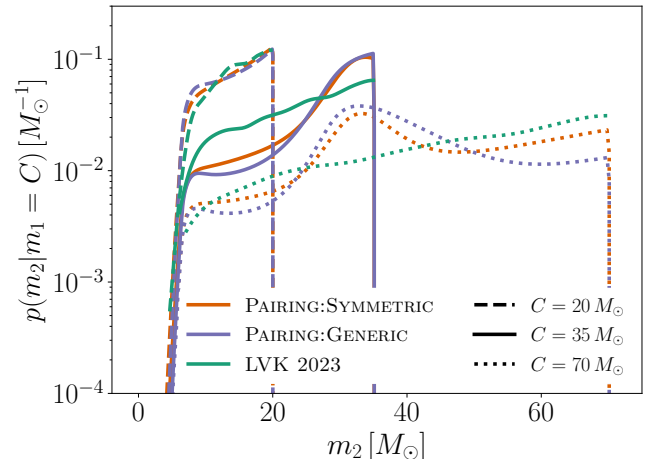


Figure 4. Conditional PPDs for the models considered in this work. We show the secondary mass distributions conditioned on $m_1 = 20 M_\odot$ (dashed), $m_1 = 35 M_\odot$ (solid) and $m_1 = 70 M_\odot$ (dotted) to exemplify when the primary mass is below, inside, and above the Gaussian peak, respectively. Colors are the same as in Figure 2. Lines denote the mean posterior probability, marginalized over hyperparameter uncertainty, and credible intervals are omitted for clarity. When m_1 is below the peak, all models agree. When m_1 is above or within the peak, PAIRING:SYMMETRIC and PAIRING:GENERIC exhibit a larger preference for m_2 to be in the peak than the LVK 2023 model does because the latter is constructed to behave like a power law in the range $[m_{\min}, m_1]$. The fact that PAIRING:GENERIC and PAIRING:SYMMETRIC approximately agree on the peak location and height indicates that the primary and secondary masses may follow the same underlying distribution up to a pairing function.

this behavior, it instead recovers similar distributions to the PAIRING:SYMMETRIC model. The Bayes factor of PAIRING:GENERIC relative to PAIRING:SYMMETRIC is $\mathcal{B}(\text{PAIRING:GENERIC})/\mathcal{B}(\text{PAIRING:SYMMETRIC}) = 0.38$, indicating an inability to distinguish between the two models, with perhaps a modest preference for the PAIRING:SYMMETRIC model.

3.2. Improved constraints on peak location

If the primary and secondary mass distributions are identical, we can better measure the properties of features in that common distribution by using measurements of both m_1 and m_2 . Figure 5 shows the one-dimensional hyperposterior for the location, μ , of the Gaussian peak in the mass distribution under the PAIRING:SYMMETRIC and LVK 2023 models. We measure μ with a standard deviation of $1.50 M_\odot$ under the PAIRING:SYMMETRIC model compared to $2.08 M_\odot$ under the LVK 2023 model, representing a 28% improvement. This increase in precision is similar to that expected from using twice the number of independent events

($1 - 1/\sqrt{2} = 0.29$), because now both m_1 and m_2 contribute to the inference, rather than just m_1 .

Furthermore, the PAIRING:SYMMETRIC model recovers a lower value of $\mu = 31.4_{-2.6}^{+2.3} M_\odot$ (median and 90% credible interval) compared to the LVK 2023 result of $\mu = 33.6_{-4.0}^{+2.6}$, because it refers to a feature in the underlying $p(m)$ distribution rather than the marginal m_1 distribution. Features in $p(m)$ appear at larger masses in the marginal m_1 distribution and lower masses in the marginal m_2 distribution due to the constraint that $m_1 > m_2$.

If the $\sim 35 M_\odot$ peak is believed to be a feature of the supernova remnant mass distribution, it is best to use its location in the underlying $p(m)$ distribution rather than its location in the marginal distribution. For example, analyses wishing to compare this feature with expectations from a pair-instability supernova pileup (e.g. Stevenson et al. 2019; Farmer et al. 2020) should use the value presented here ($\mu = 31.4_{-2.6}^{+2.3} M_\odot$). Interestingly, this lower peak location is in further tension with the latest theoretical predictions for a pair-instability pileup (Frag et al. 2022).

When possible, though, it is best to compare theoretical predictions directly to the two-dimensional mass distribution (such as those in Figure 2) rather than to the values of specific hyperparameters, since hyperparameters have different meanings in different models. Correspondingly, it is important that models used to fit the data are intentionally constructed to allow for features in both the primary and secondary mass distribution. Many of the current parametric (Fishbach & Holz 2017a; Talbot & Thrane 2018; Baxter et al. 2021; Abbott et al. 2021b, 2023a) and nonparametric (Tiwari 2021; Edelman et al. 2022a; Callister & Farr 2023; Godfrey et al. 2023)⁴ BBH mass distribution models enforce asymmetry between m_1 and m_2 , excluding the possibility that the primary and secondary mass distributions share the same features (with a few exceptions, e.g. Edelman et al. 2022b; Ray et al. 2023; Sadiq et al. 2023).

Another application of our improved measurement of the peak location is “spectral siren” cosmology, which uses such features in the mass distribution to infer the expansion history of the universe (Chernoff & Finn 1993; Messenger & Read 2012; Taylor et al. 2012; Farr et al. 2019; Ezquiaga & Holz 2021, 2022; Abbott et al. 2023b).

⁴ Callister & Farr (2023) and Godfrey et al. (2023) use flexible models to fit $p(q)$ rather than using power laws, but they do not use a pairing function and instead fit the m_1 and q distributions independently, therefore assuming the product of the marginal distributions equals the two-dimensional distribution. This is the same fundamental choice as is described in Equation A1, and therefore assumes that m_1 and m_2 follow different distributions.

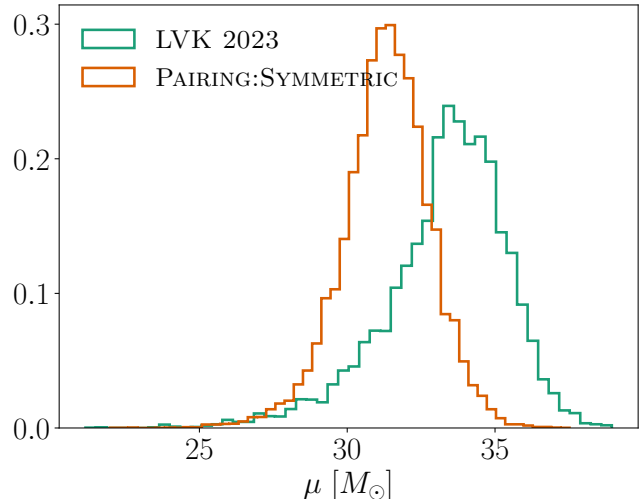


Figure 5. Marginal posteriors on μ , the location of the Gaussian peak, for the LVK 2023 and PAIRING:SYMMETRIC models. This parameter is more precisely measured under the PAIRING:SYMMETRIC formalism by $\sim 1/\sqrt{2}$, indicating that m_1 and m_2 independently contribute to this measurement. μ is the most correlated parameter with the Hubble constant when using “spectral sirens” (Ezquiaga & Holz 2022; Abbott et al. 2023b), so using the PAIRING:SYMMETRIC model will presumably improve cosmological measurements. The central values of the two distributions differ because the hyperparameter performs has slightly different effects on the resulting 2D mass distribution each model.

Previous analyses found the location of this peak to be the parameter most correlated with the Hubble constant (see Figures 5 and 13 of Abbott et al. 2023b), so an improved constraint on μ should therefore have a relatively large effect on the constraints of cosmological parameters if all other mass distribution parameters remain equally-well constrained.

3.3. Evidence for a peak in the secondary mass distribution

Consistency between the primary and secondary mass distributions implies a peak in the secondary mass distribution at $m_2 \sim 30 M_\odot$, as this feature has already been robustly identified in the primary mass distribution (Abbott et al. 2021b; Tiwari 2021; Abbott et al. 2023a; Edelman et al. 2022b; Callister & Farr 2023; Farah et al. 2023). However, the data is also consistent with differing primary and secondary mass distributions, as shown by the regions in which the filled and dashed bands do not overlap in Figure 3. In this case, it is worthwhile to explicitly determine whether there exists a peak in the secondary mass distribution.

The left panel of Figure 6 shows the posterior distribution for the parameters governing the height of the peak in m_1 and m_2 under the PAIRING:GENERIC model, λ_1

and λ_2 , respectively. Setting $\lambda_{\{1,2\}} = 0$ means that no binaries in the astrophysical population are in the Gaussian peak⁵, while $\lambda_{\{1,2\}} = 1$ means all binaries are in the Gaussian peak. The lower left and upper right regions of the two-dimensional posterior are excluded, meaning that λ_1 and λ_2 cannot both be zero, nor can they both be large. This indicates that either one of the two distributions has a large peak while the other has none, or that both distributions have moderate peaks.

In fact, the posterior on λ_2 peaks at a higher value than λ_1 . Under the LVK 2023 model, the 1D posterior on λ peaks between the marginal λ_1 and λ_2 posteriors of the PAIRING:GENERIC model. Additionally, in the PAIRING:GENERIC model, λ_1 has more support at zero relative to λ , while λ_2 has reduced support at zero. This hints at the intriguing possibility that the secondary masses may be driving the nonzero value of λ found by Abbott et al. (2021b) and Abbott et al. (2023a). In other words, *it is possible that the $\sim 30 M_\odot$ peak exists the secondary mass distribution rather than the primary mass distribution.* However, the data are still consistent with $\lambda_1 = \lambda_2$: the dashed grey line in Figure 6 intersects the 1.5- σ contour of the hyperposterior.

As shown in Appendix A.3, the LVK 2023 formalism behaves similarly to PAIRING:NO PEAK IN $p_2(m_2)$, which is nested within PAIRING:GENERIC when $\lambda_2 = 0$. Therefore, ruling out $\lambda_2 = 0$ would indicate that the pairing function formalism is strongly preferred. We find that $\lambda_2 = 0$ is disfavored but not ruled out: there is 4.2 times more posterior density at $\lambda_2 = 0.17$ (its median *a posteriori* value) than at $\lambda_2 = 0$. It is therefore difficult to tell with the current number of detections whether the data prefer for the peak to exist in $p_1(m_1)$, $p_2(m_2)$, or both.

These possibilities are somewhat degenerate because of the preference for equal mass BBHs. To illustrate this, the right panel of Figure 6 compares the power law spectral index, β_q , of the pairing function under PAIRING:GENERIC and PAIRING:NO PEAK IN $p_2(m_2)$. When there is no peak in $p_2(m_2)$, the β_q posterior shifts to higher values, which corresponds to a larger preference for $q \sim 1$. This is because the PAIRING:NO PEAK IN $p_2(m_2)$ model has a peak in $p_1(m_1)$, so it allows for a high fraction of secondary masses to lie within the peak by making more binaries equal-mass. For comparison, we also plot the posterior on β_q under PAIR-

ING:SYMMETRIC to show how a different set of assumptions about λ_2 changes β_q . The shift in β_q when $\lambda_2 = 0$ is larger than when $\lambda_2 = \lambda_1$, suggesting that it is driven by an excess of events with $m_2 \sim 35 M_\odot$ rather than by other model assumptions or a different realization of the inference.

In summary, we find modest evidence for a peak in $p_2(m_2)$, suggesting that pairing function models may be preferred over the LVK 2023 formalism, though current observations do not allow us to definitively rule out that the peak exists only in $p_1(m_1)$. The data is consistent with $\Lambda_1 = \Lambda_2$, so there is not strong evidence against the possibility that m_1 and m_2 are drawn from the same underlying distribution, up to a pairing function.

3.4. Binary black holes are picky

Pairing functions provide an intuitive way to quantify whether the properties of one black hole in a binary influences those of its companion. Binaries that pair up independently of each component's masses are described by a pairing function with $\beta_q = 0$, whereas a preference for equal-mass binaries is described by $\beta_q > 0$. We find $\beta_q > 0$ to $> 99.99\%$ for PAIRING:SYMMETRIC and to 99.95% for PAIRING:GENERIC. This is consistent with an earlier study by Fishbach & Holz (2020) who use the pairing function formalism on GWTC-1 (Abbott et al. 2019). However, BBHs are not maximally picky: the posterior on β_q is not railing against the high end of the prior bounds.

Our inferred two-dimensional mass distribution is generally consistent with that shown in Sadiq et al. (2023), who use a non-parametric approach and assume that the population is symmetric under $m_1 \leftrightarrow m_2$. They show evidence for peaks in the mass ratio distribution at $q \sim 0.5$ when $m_1 \sim 15 M_\odot$ and $m_1 \sim 70 M_\odot$, which they interpret as a lack of preference for similar-mass pairings. However, we note that these peaks in the mass ratio distribution translate to peaks in the secondary mass distribution at $\sim 7 M_\odot$ and $\sim 35 M_\odot$, the same locations at which the primary mass distribution exhibits peaks. Parametrizations that assume symmetry under $m_1 \leftrightarrow m_2$ but do not use a pairing function are unable to disentangle the effects of preference for similar-mass pairings from features in one or both component mass distributions. We therefore conclude that both our results and those presented in Sadiq et al. (2023) are consistent with a preference for similar-mass pairings as well as structure in the secondary mass distribution.

In this work, we have only examined power law forms for the pairing function, but more complex models are under investigation and will be presented in future work. If the pairing function is a more complex function of

⁵ The integrated fraction of events in the region near the peak is higher than the fraction indicated by λ because both the Gaussian peak and the underlying power law contribute to the rate in that region. Therefore, $\lambda_{\{1,2\}} = 0$ does not mean that there are no events with masses $\sim 35 M_\odot$.

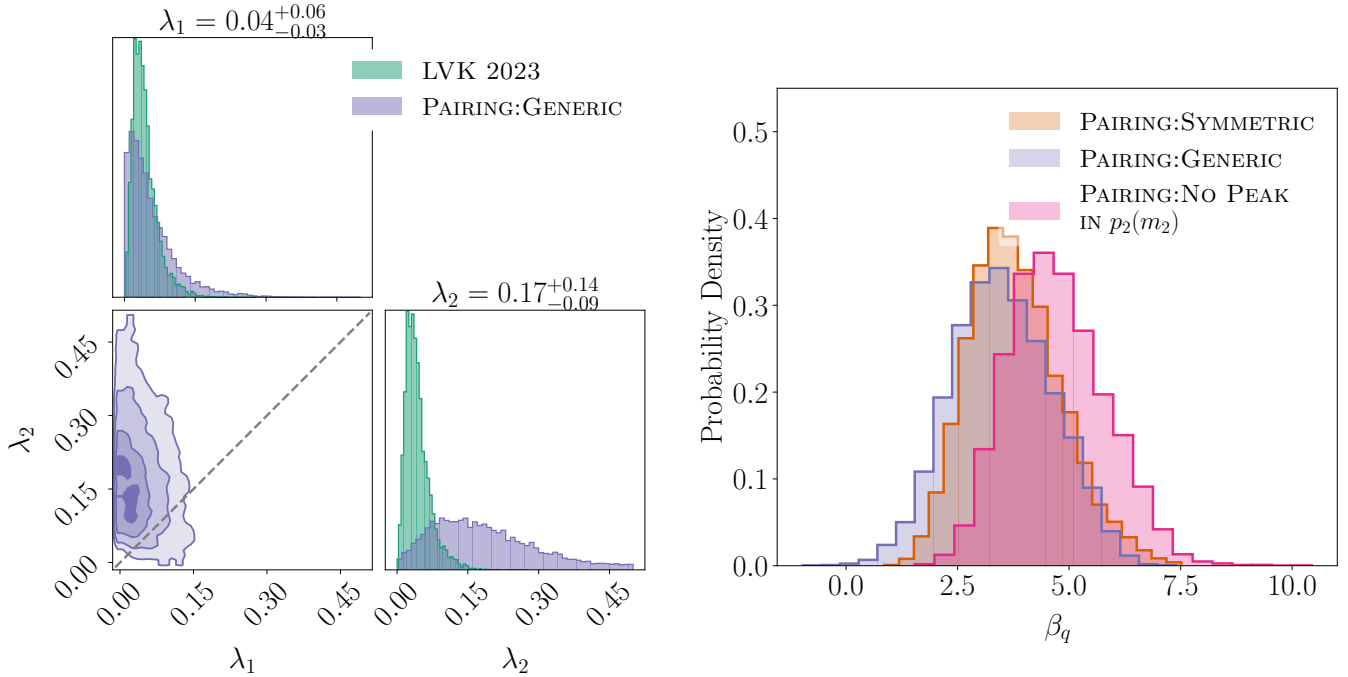


Figure 6. Hyperposteriors under pairing function models. *Left:* Corner plot of hyperparameters governing the height of the Gaussian peak for the primary (λ_1) and secondary (λ_2) mass distributions under the PAIRING:GENERIC model. The medians and 90% credible intervals are shown over their respective marginal distributions. The medians indicate that roughly 17% of BBHs have secondary masses in the Gaussian peak while 4% have primary masses in the peak, though this preference for a larger peak in $p_2(m_2)$ may be due to the relatively poor constraint on λ_2 rather than a real preference of the data. The lower left portion of the two-dimensional posterior is excluded, indicating that there must be a peak in either $p_1(m_1)$ or $p_2(m_2)$, and a slight preference exists for the peak to be in $p_2(m_2)$ (upper left portion of plot) or both distributions (central portion of plot), though the peak being in $p_1(m_2)$ only is not ruled out. For reference, the 1D posterior on λ under the LVK 2023 model is shown in green, with $\lambda = 0.04_{-0.02}^{+0.03}$ (Abbott et al. 2023a). The dashed grey line indicates where $\lambda_1 = \lambda_2$. *Right:* Marginal posteriors on β_q , the hyperparameter controlling the steepness of the pairing function under the PAIRING:SYMMETRIC, PAIRING:GENERIC, and PAIRING:NO PEAK IN $p_2(m_2)$ models. When we set $\lambda_2 = 0$, β_q increases, indicating a preference for equal-mass components. This behavior is likely caused to accommodate an excess of events with $m_2 \sim 35 M_\odot$, which can either be caused by a peak in $p_2(m_2)$ or with a peak in $p_1(m_1)$ and a strong preference for equal-mass binaries (see discussion in Appendix A.1).

mass ratio, or if it depends on multiple parameters, such as primary mass or spin (e.g. Farah et al. 2022), it may become easier to distinguish between pairing function models and models parameterized similarly to LVK 2023, as complex pairing functions may find more support away from the $m_1 = m_2$ diagonal. The same is true if the marginal mass ratio distribution has multiple modes, or if mass ratio is allowed to correlate with other parameters (e.g. effective spin, Callister et al. 2021).

4. LOOKING TO THE FUTURE

The LVK 2023 and pairing function models differ most in their predictions for the number of events in the region $m_1 \in [35, 40] \cap m_2 \in [m_{\min}, 30]$, because they disagree on whether to place m_2 in the Gaussian peak or somewhat evenly throughout the available parameter space. We can therefore determine which model will be preferred in the future by counting the number of detected events in that region.

It is expected that 260_{-150}^{+330} BBHs will be detected by the end of the LVK’s fourth observing run (O4), and 870_{-480}^{+1100} BBHs will be detected by the end of the fifth observing run (O5) (Kiadrebeogo et al. 2023). With 260 (870) total BBH detections, we expect 23.6 ± 4.6 (79.0 ± 8.5) BBHs to fall in the region $m_1 \in [35, 40] \cap m_2 \in [m_{\min}, 30]$ under the LVK 2023 model and 12.6 ± 3.5 (42.3 ± 6.3) under the PAIRING:SYMMETRIC model. This means that by the end of O4, we will be able to distinguish the LVK 2023 and PAIRING:SYMMETRIC models to $> 2\sigma$, and we can distinguish them to $> 4\sigma$ by the end of O5.

Of course, it is necessary to perform a full hierarchical analysis, as measurement uncertainties of detected systems will cause events to scatter into and out of this region. Additionally, in a hierarchical Bayesian context, posterior predictive checks performed on the event-level parameters (such as the true masses of individual events) are less sensitive than those performed on the *observed*

data (Sinharay & Stern 2003; Gelman 2006; Bayarri & Castellanos 2007; Loredo 2013). This is why, for example, Fishbach et al. (2020) performs posterior predictive checks on the maximum-likelihood values of the observed and predicted events. Therefore, more sensitive posterior predictive checks may be able to distinguish between the two frameworks with fewer events than we project here.

5. SUMMARY AND IMPLICATIONS FOR ASTROPHYSICS OF MERGING BBHS

We explored whether the primary and secondary component masses in merging BBHs are drawn from the same distribution, or whether the BBH mass distribution is asymmetric in $m_1 \leftrightarrow m_2$, as is commonly assumed in BBH population studies. Comparing these two possibilities for the first time, we determine that m_1 and m_2 are consistent with being drawn from the same underlying BH mass distribution. In particular, we find that a peak likely exists in the secondary mass distribution at the same location as the $\sim 35 M_\odot$ peak previously identified in the primary mass distribution. This finding has implications for the formation channels of merging BBHs and the origin of the $\sim 35 M_\odot$ peak.

If the mass distribution is indeed symmetric under $m_1 \leftrightarrow m_2$ as in our preferred model PAIRING:SYMMETRIC, this may imply that a large fraction of merging BBHs are formed through dynamical assembly, in which the two component BHs are born through a similar process and find each other in a dense stellar environment. In this case, the pairing function and its dependence on mass ratio and/or total mass may encode valuable information about dynamical processes like mass segregation and binary exchanges.

The appearance of a peak in both primary and secondary mass distributions is consistent with an origin in the BH remnant mass function. However, the peak location at $31.4_{-2.6}^{+2.3} M_\odot$ is in tension with predictions for pair-instability supernovae. As another application of our work, we suggest that future spectral siren measurements consider the PAIRING:SYMMETRIC model when inferring the Hubble constant, because it provides an improved measurement of the peak location relative to the LVK 2023 model and the peak location is strongly correlated with the inferred value of H_0 .

On the other hand, the data remain consistent with an asymmetric BBH mass distribution $p(m_1, m_2)$, in which $p_1(m_1) \neq p_2(m_2)$, as in the PAIRING:GENERIC model. This would imply that a significant fraction of merging BBHs originate from field binaries, in which “primary” and “secondary” are physically meaningful if they tend to correspond to the first-born or second-

born BH in a binary. The component mass distributions $p_1(m_1)$ and $p_2(m_2)$ would then encode the binary IMF and the highly uncertain physics of binary stellar evolution. Specifically, the location and prominence of features in each component mass distribution may provide insight into how mass loss versus mass accretion affect stellar evolution and collapse, including their effect on supernovae and the BH remnant mass function.

Notably, if the BBH mass distribution is asymmetric, we find that *it is possible that no peak exists in the primary mass distribution, and the previously-identified peak in primary mass is actually driven by an overdensity in the secondary mass distribution.* A peak that is more prominent in $p_2(m_2)$ than $p_1(m_1)$ may imply that pulsational pair-instability supernovae are more frequent or are shifted to lower masses among second-born BHs.

Additionally, the degree of asymmetry in the BBH mass distribution provides insight into the frequency of mass inversion in binary stars, providing a complementary probe to BH spins (Mould et al. 2022). If mass inversion never occurs, m_1 will typically be the remnant of the donor star. However, if mass inversion is the norm, m_1 will be the remnant of the accretor star. A perfectly symmetric BBH distribution under isolated binary evolution would imply that mass inversion happens exactly 50% of the time, causing the primary and secondary mass distributions to be indistinguishable even though binary physics imparts different distributions on the first-born versus second-born black hole, but this is statistically unlikely.

We additionally find that BHs in merging binaries have a strong preference to pair with similar-mass BHs for all forms of the secondary mass distribution considered in this work. This is consistent with the results presented in Fishbach & Holz (2020), though we more confidently exclude the scenario in which BBHs pair independently of mass ratio since we now have many more detected BBHs.

By the end of the LVK’s fifth observing run, we expect to confidently distinguish between the different scenarios presented here for the BBH mass distribution. In this work, we found that secondary masses in merging BBH systems likely display a peak at $\sim 35 M_\odot$, whereas previous results identified this peak exclusively among primary masses. With a few hundred additional BBH observations, we expect to determine whether both component mass distributions have a peak at the same location or the peak is more prominent among secondary masses.

Facilities: LIGO, Virgo

Software: `gwpopulation` (Talbot et al. 2019), `bilby` (Ashton et al. 2019), `scipy` (Virtanen et al. 2020), `corner.py` (Foreman-Mackey 2016)

1 The authors thank Sharan Banagiri, Thomas Dent, Zo-
 2 heyr Doctor, Will Farr, Davide Gerosa, Tom Loreda,
 3 and Jam Sadiq for helpful discussions. A.M.F. is sup-
 4 ported by the National Science Foundation Graduate
 5 Research Fellowship Program under Grant No. DGE-
 6 1746045. D.E.H is supported by NSF grants AST-
 7 2006645 and PHY-2110507, as well as by the Kavli In-
 8 stitute for Cosmological Physics through an endowment
 9 from the Kavli Foundation and its founder Fred Kavli.
 10 This research has made use of data or software ob-
 11 tained from the Gravitational Wave Open Science Cen-
 12 ter (`gwosc.org`), a service of the LIGO Scientific Col-
 13 laboration, the Virgo Collaboration, and KAGRA. This
 14 material is based upon work supported by NSF’s LIGO
 15 Laboratory which is a major facility fully funded by the
 16 National Science Foundation. The authors are grateful
 17 for computational resources provided by the LIGO Lab-
 18 oratory and supported by National Science Foundation
 19 Grants PHY-0757058 and PHY-0823459.

APPENDIX

A. COMPARISON WITH COMMON PARAMETRIZATIONS

A.1. Differences between mass distribution parametrizations

Given a form for the primary mass distribution, there are several ways to construct a two-dimensional mass distribution. We discuss two possibilities here that are common in the literature, showing the different effects they have on the resulting two-dimensional mass distribution.

The main qualitative differences between the two parametrizations are illustrated in Figure 7. The top row has three examples of mass distributions that can be described by a model of the form

$$p(m_1, m_2 | \Lambda_m, \beta) = p(m_1 | \Lambda_m) p(q | m_1, m_{\min}, \beta) \quad (\text{A1})$$

for different values of β . Here, m_1 is the mass of the heavier component in the binary, m_2 is the mass of the lighter component, and $q = m_2/m_1 \leq 1$ is the mass ratio. This can be equivalently written as

$$p(m_1, m_2 | \Lambda_m, \beta) = p(m_1 | \Lambda_m) p(m_2 | m_1, \beta), \quad (\text{A2})$$

since $m_2 = qm_1$. The parametrization described in Equation A1 is used by all parametric models presented in Abbott et al. (2021b) and Abbott et al. (2023a) that were used to model the primary mass distribution of BBHs, such as BROKEN POWER LAW and POWER LAW + PEAK, and is also commonly used in other analyses (e.g., Fishbach & Holz 2017a; Kovetz et al. 2017; Talbot & Thrane 2018; Tiwari 2021; Edelman et al. 2022a; Callister & Farr 2023; Godfrey et al. 2023). For the remainder of this Appendix, we will refer to models parameterized by Equation A1 as “CONDITIONED-Q,” since they require the mass ratio distribution to be explicitly conditioned on primary mass.

The bottom row of Figure 7 has three examples of mass distributions that can be described using a “pairing function”, f (Fishbach & Holz 2020). Models with pairing functions have the form

$$p(m_1, m_2 | \Lambda) = p_1(m_1 | \Lambda_1) p_2(m_2 | \Lambda_2) f(q; \beta_q) \quad (\text{A3})$$

where $f(q)$ is a pairing function that depends on the mass ratio of the system⁶, and $\Lambda = \{\Lambda_1, \Lambda_2, \beta_q\}$ is the set of all model hyperparameters. In this work, we use a pairing function of the form $f(q; \beta_q) = q^{\beta_q} \Theta(q \leq 1)$, though other

⁶ In principle, the pairing function can be parameterized in terms of any observable parameter (e.g., total mass).

forms may provide a better fit to the data (e.g. Farah et al. 2022). In the examples illustrated in Figure 7, the primary and secondary mass distributions are equivalent, so $p_1(m) = p_2(m) \equiv p(m)$. Alternatively, $\Lambda_1 = \Lambda_2$. This describes a situation in which there is a single underlying mass distribution from which both components are drawn. The pairing function then describes how likely the two components are to be combined in a merging binary based on their mass ratio. A pairing function that prefers equal mass binaries will cause a marginal mass ratio distribution that has more support near $q = 1$, but the inverse is not necessarily true.

The parametrization in Equation A3 factorizes the possibility that components in binaries prefer to be near-equal mass and the possibility that the primary and secondary masses have distinct probability distributions. In other words, pairing functions allow us to model the secondary mass separately from the primary mass, while also allowing for the possibility that component BHs prefer to pair with similar-mass BHs.

In Figure 7, a peak at $35 M_\odot$ is placed in both models to show the effects of such features in both cases. One consequence of CONDITIONED-Q models is that features such as Gaussian peaks can only appear in the primary mass distribution. This is shown by the vertical bands in the top row of Figure 7 and lack of horizontal bands, since a band in the vertical (horizontal) direction are caused by a peak or dip in the primary (secondary) mass distribution for a range of secondary (primary) masses. For pairing function models, features can appear in $p_1(m_1)$, $p_2(m_2)$, or both. We have illustrated the case in which the same feature appears in both component mass distributions, and this appears as both the vertical and horizontal bands in the bottom row of Figure 7. If Λ_1 and Λ_2 are allowed to differ, features could appear in only one of these distributions. This would cause there to only be horizontal bands if features only existed in $p_2(m_2)$, and only vertical bands if features only existed in $p_1(m_1)$. Features are also able to appear in different locations in $p_1(m_1)$ vs $p_2(m_2)$ under the pairing function formalism. However, the CONDITIONED-Q formalism only allows for bands in the vertical direction, meaning that it is not flexible enough to capture true underlying distributions with features in $p_2(m_2)$. The behavior of the CONDITIONED-Q formalism can in general be approximated by the pairing function formalism, while the opposite is not true.

The different columns in Figure 7 correspond to different power law spectral indices for the mass ratio distribution (*top row*, β) and mass ratio-dependent pairing function (*bottom row*, β_q). The top row’s leftmost panel has a uniform mass ratio distribution, the middle panel has a mass ratio distribution that mildly favors equal-mass binaries, and the right panel’s mass ratio distribution strongly favors equal mass binaries. Analogously, the bottom row’s leftmost panel shows a model where components in the binary are allowed to pair up independently of mass ratio, the middle panel shows a model where components have a slight preference to pair up with partners that are equal mass, and the rightmost panel shows the case where components are “picky”: they almost always pair up with equal mass partners (Fishbach & Holz 2020). When the mass ratio distribution is broad, or when components pair near-independently of mass ratio, the CONDITIONED-Q models produce noticeably different distributions than the pairing function models. However, in the case of very picky binaries or a steeply rising mass ratio distribution, the CONDITIONED-Q and pairing function models become difficult to tell apart, and likely explain the data equally well. There is therefore a degeneracy between the steepness of the pairing function and the existence of distinct features in the two mass distributions (see Tiwari 2023, for a discussion of this phenomenon in terms of Jacobian transformations).

Fortunately, as we will show in Section 3.4, we measure $\beta \sim 3.5$ and $\beta_q \sim 1$, so the data lie somewhere between the middle and rightmost columns.⁷ This means that differentiating between the two scenarios will be difficult, but possible given enough data.

Mass distributions of compact objects are often visualised through a plot of the marginal component mass distributions. The marginal m_2 distribution is defined as

$$p(m_2|\Lambda) = \int dm_1 p(m_1, m_2|\Lambda), \quad (\text{A4})$$

where $p(m_1, m_2|\Lambda)$ can be parameterized in the way described in Equation A1 or Equation A3. However, in all but the top left panel in Figure 7, the *marginal* secondary mass distribution exhibits a peak between $30 M_\odot$ – $40 M_\odot$, even though the secondary mass distribution is not able to have any features on its own. This is because features in the primary mass distribution induce features in the marginal secondary mass distribution if equal-mass binaries are

⁷ The value for β under CONDITIONED-Q is different than the value found for β_q under the pairing function models because the two parameters cause different behaviors in the 2D mass distribution within their respective models. A low value for β does not imply that BBHs are not picky, just that the marginal mass ratio distribution rises slowly. We discuss this in more detail in Appendix A.2.

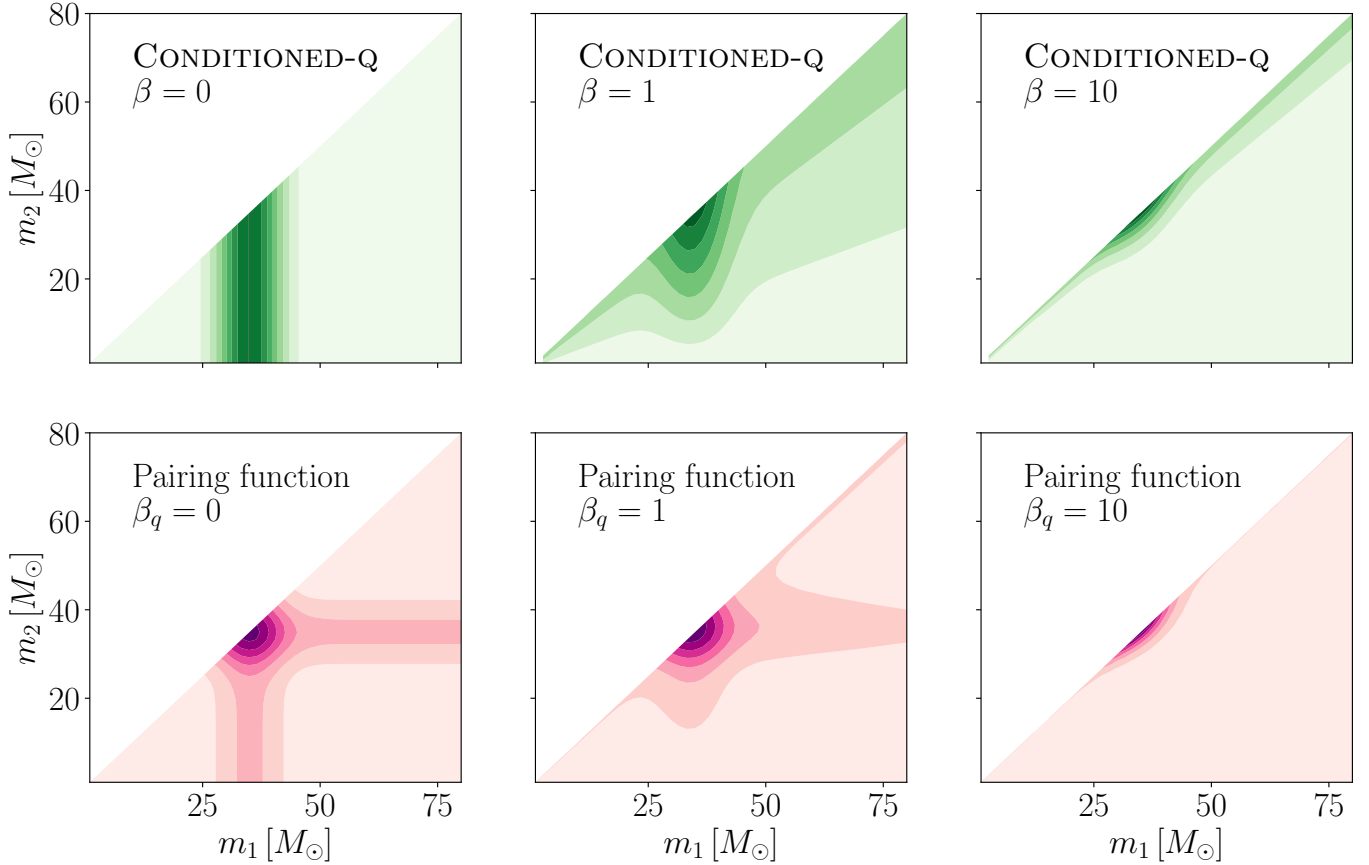


Figure 7. Illustration of some possible two-dimensional mass distributions under the commonly used “CONDITIONED-Q” formalism described by Equation A1 (*top row*) and the pairing function formalism described by Equation A3 (*bottom row*). Overdensities/peaks in the mass distribution appear as darker filled contours in these figures. The CONDITIONED-Q formalism is only able to produce models with features in the m_1 distribution, as shown by the vertical bands in the top row, whereas the pairing function formalism can model features in either m_1 or m_2 , or both. The different columns correspond to different power law spectral indices for the mass ratio distribution (*top row*, β) and mass ratio-dependent pairing function (*bottom row*, β_q). In the case of a steeply rising mass ratio distribution, or if components strongly prefer to pair with nearly equal-mass partners, the CONDITIONED-Q model and the pairing function model become difficult to tell apart and likely explain the data equally well, as shown by the two panels in the leftmost column. The diagonal contours in the middle and right columns are caused by a preference for equal-mass binaries and follow lines of constant mass ratio.

preferred: when a binary’s primary mass is within the peak, its secondary mass is also likely to be in that peak simply because $m_2 \simeq m_1$ is preferred. It is therefore difficult to distinguish between these different scenarios by looking at the marginal distributions alone. Instead, we analyze two-dimensional distributions such as the ones illustrated in Figure 7, as well as the secondary mass distributions conditioned at various values of m_1 . The latter can be thought of as one-dimensional slices of the former.

It is our goal to determine whether the data prefer models described by pairing functions or by CONDITIONED-Q functions. We also aim to determine if the primary and secondary masses are drawn from the same distribution, and whether we can draw physical insights from features that appear in the primary mass distribution, secondary mass distribution, or both.

A.2. Mass ratio distributions vs. pairing functions

Under the CONDITIONED-Q formalism, we cannot determine how BHs in binaries choose their companions, though we can gain some insight from their marginal mass ratio distribution. CONDITIONED-Q parametrizes the mass ratio distribution as a power law with spectral index β , where $\beta > 0$ corresponds to mass ratio distributions with more support for similar-mass binaries. Abbott et al. (2023a) find $\beta = 1.1^{+1.7}_{-1.3}$, which similarly indicates a preference for

equal-mass binaries. Note that the value for β under CONDITIONED-Q is noticeably different than the value found for β_q under the pairing function models because the two parameters cause different behaviors in the 2D mass distribution within their respective models. A low value for β does not imply that BBHs are not picky, just that the marginal mass ratio distribution rises slowly. As shown in Appendix B.3, the pairing function models and CONDITIONED-Q model all produce near-identical marginal mass ratio distributions, despite different values for β_q and β . Low values for β are partially due to the fact that the low- q end of the marginal mass ratio distribution will always be suppressed because of the existence of a minimum BH mass. This minimum mass makes it impossible to get extreme mass ratios unless m_1 is very large, and the m_1 distribution has very little support for $m_1 \gtrsim 60 M_\odot$. Therefore, β does not need to be large in order for the marginal mass ratio distribution to strongly disfavor unequal-mass binaries. In fact, the existence of a minimum mass plus a tapering at high m_1 means that even when $\beta < 0$, the marginal mass ratio distribution rises towards $q = 1$.

A.3. Mimicking CONDITIONED-Q with a pairing function model

We show that the PAIRING:NO PEAK IN $p_2(m_2)$ model approximates the morphology of the LVK 2023 model, which uses the CONDITIONED-Q formalism.

The right two panels of Figure 11 show the two-dimensional PPDs for the LVK 2023 and PAIRING:NO PEAK IN $p_2(m_2)$ models. Both exhibit vertical bands and no horizontal bands, and have a similar-magnitude drop in merger rate moving away from the diagonal.

The leftmost panel of Figure 11 shows the conditional m_2 distribution for both models. While the slopes of the two models differ slightly, a peak in m_2 appears in neither. We therefore find PAIRING:NO PEAK IN $p_2(m_2)$ to be an appropriate proxy for the behavior of the LVK 2023 model for the purposes of this work. A future measurement ruling out $\lambda_2 = 0$ with high confidence would therefore serve as evidence for the pairing function models over LVK 2023-like models.

B. GENERAL POPULATION MODEL

B.1. Base model

We model the two-dimensional mass distribution by constructing separate one-dimensional distributions for the primary and secondary masses and combining draws from these two distributions according to a pairing function, as in Equation A3. Fishbach & Holz (2020) find the pairing function is most informative when parameterized by the mass ratio of the binary, so we adopt a pairing function described by a power law in mass ratio.

Because our aim is to learn whether the primary and secondary masses are consistent with being drawn from the same distribution (up to a pairing function and subject to the constraint that $m_1 \geq m_2$), we describe the primary and secondary mass distributions separately, but according to the same functional form. We model each of the 1-dimensional mass distributions as a mixture model between a smoothed power law component and a Gaussian component G in order to make direct comparisons to the POWER LAW + PEAK model used by the LIGO-Virgo-KAGRA's (LVK) population analysis to describe the distribution of primary masses Talbot & Thrane (2018); Abbott et al. (2023a). Explicitly,

$$\begin{aligned}
 p(m_1|\Lambda_1) &\propto \left[(1 - \lambda_1)\Theta(m_1 > m_{\min,1})\Theta(m_1 < m_{\max,1}) \left(\frac{\alpha_1 + 1}{m_{\max,1}^{\alpha_1+1} - m_{\min,1}^{\alpha_1+1}} \right) m_1^{-\alpha_1} + \lambda_1 G(m_1|\mu_1, \sigma_1) \right] \\
 &\quad \times S(m_1|m_{\min,1}, \delta_1) \\
 p(m_2|\Lambda_2) &\propto \left[(1 - \lambda_2)\Theta(m_2 > m_{\min,2})\Theta(m_2 < m_{\max,2}) \left(\frac{\alpha_2 + 1}{m_{\max,2}^{\alpha_2+1} - m_{\min,2}^{\alpha_2+1}} \right) m_2^{-\alpha_2} + \lambda_2 G(m_2|\mu_2, \sigma_2) \right] \\
 &\quad \times S(m_2|m_{\min,2}, \delta_2).
 \end{aligned} \tag{B5}$$

Here, $G(m_{\{1,2\}}|\mu_{\{1,2\}}, \sigma_{\{1,2\}})$ is a normalized Gaussian distribution with mean $\mu_{\{1,2\}}$ and width $\sigma_{\{1,2\}}$. The parameter $\lambda_{\{1,2\}}$ is a mixing fraction determining the relative prevalence of mergers the power law and Gaussian components, and $S(m_{\{1,2\}}, m_{\min,\{1,2\}}, \delta_{\{1,2\}})$ is a smoothing function which rises from 0 to 1 over the interval $(m_{\min,\{1,2\}}, m_{\min,\{1,2\}} + \delta_{\{1,2\}})$. Λ_1 is then the set of hyperparameters $\{m_{\min,1}, m_{\max,1}, \alpha_1, \lambda_1, \mu_1, \sigma_1, \delta_1\}$ and $\Lambda_2 = \{m_{\min,2}, m_{\max,2}, \alpha_2, \lambda_2, \mu_2, \sigma_2, \delta_2\}$.

In all models considered in this work, the redshift distribution is modeled as a power law with spectral index κ (Fishbach et al. 2018) such that

$$p(z) \propto \frac{dV_c}{dz} \left(\frac{1}{1+z} \right) (1+z)^\kappa. \quad (\text{B6})$$

We use the DEFAULT spin model from Abbott et al. (2021b, 2023a) to describe the spin magnitudes and tilts of each component. These are the same redshift and spin distributions used with the POWER LAW + PEAK mass model in the analysis presented in Abbott et al. (2023a).

A fit to the model described above is provided in Appendix B, though we focus on specific variations nested within this more general model for the remainder of this work.

B.2. Fit to General Base Model

We present results of a fit to the most general form of the pairing function model described in Section B.1 (Equation B5). Here, we do not fix any parameters to be equal between Λ_1 and Λ_2 , and instead infer them separately.

Figure 8 shows the posterior of all mass-related hyperparameters within this model in the form of a corner plot. Because of the large number of free parameters, several are not well-constrained. Nonetheless, all parameters describing $p_1(m_1)$ are consistent with those describing $p_2(m_2)$. Additionally, strong correlations exist between α_1, α_2 , and β_q , making it difficult to meaningfully constrain all three parameters. We therefore set $\alpha_1 = \alpha_2$ in the PAIRING:GENERIC model.

Figure 9 shows the underlying distributions, $p_1(m_1)$ and $p_2(m_2)$ inferred by the most general version of the base model. As expected, the constraints on these distributions weaken relative to that of the PAIRING:GENERIC model. However it is still clear that $p_1(m_1)$ and $p_2(m_2)$ are consistent with one another and that it is possible that $p_2(m_2)$ has a larger peak than $p_1(m_1)$ does. Notably, there now seems to be very little evidence for a peak in $p_1(m_1)$, whereas a clear peak still exists in $p_2(m_2)$.

These results are consistent with what has been presented using the PAIRING:GENERIC model in the main body of this work.

B.3. Model Comparison

In this Section, we compare the various models considered in this work, including the CONDITIONED-Q model. Table 1 lists the hyperprior choices made to construct each model, along with descriptions of each hyperparameter.

Figure 10 shows the m_1 , m_2 , and q PPDs, marginalized over all other parameters. These show a high level agreement between the different models, despite their two-dimensional PPDs differing in Figure 2. Notably, the marginal secondary mass distribution exhibits a peak even for the CONDITIONED-Q model. As discussed in Appendix A.1, this is caused by the preference for equal masses: if m_1 is in the $\sim 35 M_\odot$ peak, a preference for $m_2 \approx m_1$ will cause m_2 to also preferentially be in that region, causing more probability density for $m_2 \sim 35 M_\odot$ than elsewhere. Marginal PPDs are therefore not very sensitive to whether m_2 prefers its own features independently of the existence of a preference for equal mass binaries. Instead, we examine the underlying component mass distributions explicitly modeled by PAIRING:SYMMETRIC and PAIRING:GENERIC, as well as the values of informative hyperparameters in these models to determine whether $p_2(m_2)$ differs from $p_1(m_1)$. For comparisons to CONDITIONED-Q, we plot secondary mass distributions conditioned on various values of m_1 .

C. STATISTICAL FRAMEWORK

In this Appendix, we describe the hierarchical Bayesian analysis used to fit the population models described in Appendix B and Section 2 to BBHs in GWTC-3 (Abbott et al. 2021a, 2023c).

The posterior on the population hyper-parameters, assuming a prior on the overall rate of mergers $p(\mathcal{R}) \sim 1/\mathcal{R}$ and marginalizing, is

$$p(\Lambda|\{D_j\}) = p(\Lambda) \prod_j^N \frac{p(D_j|\Lambda)}{\mathcal{E}(\Lambda)}, \quad (\text{C7})$$

where

$$p(D_j|\Lambda) = \int dm_1 dm_2 ds_1 ds_2 dz p(z) p(s_1, s_2) p(m_1, m_2|\Lambda) p(D_j|m_1, m_2, s_1, s_2, z) \quad (\text{C8})$$

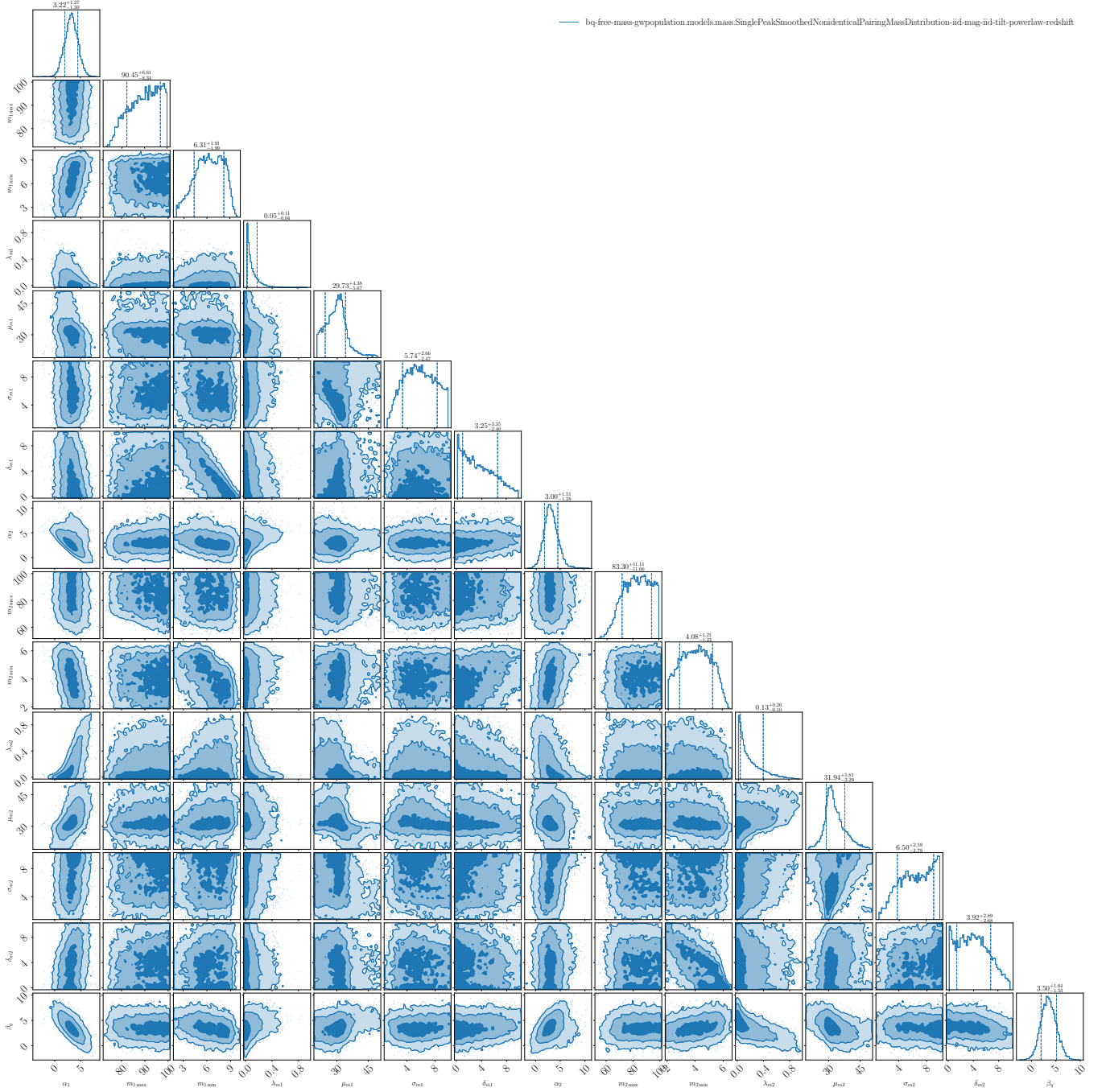


Figure 8. Corner plot of all mass-related hyperposteriors in the most general form of the base model. Power law spectral indices governing the slope of the primary and secondary mass distributions are degenerate with one another and with the pairing function power law, so only two of the three parameters can be meaningfully constrained at a time. All other parameters that perform the same function in $p_1(m_1)$ and $p_2(m_2)$ are consistent between the two underlying distributions.

is the marginal likelihood for the j^{th} event,

$$\mathcal{E}(\Lambda) = \int dm_1 dm_2 ds_1 ds_2 dz p(z) p(s_1, s_2) p(m_1, m_2 | \Lambda) P(\det | m_1, m_2, s_1, s_2, z) \quad (\text{C9})$$

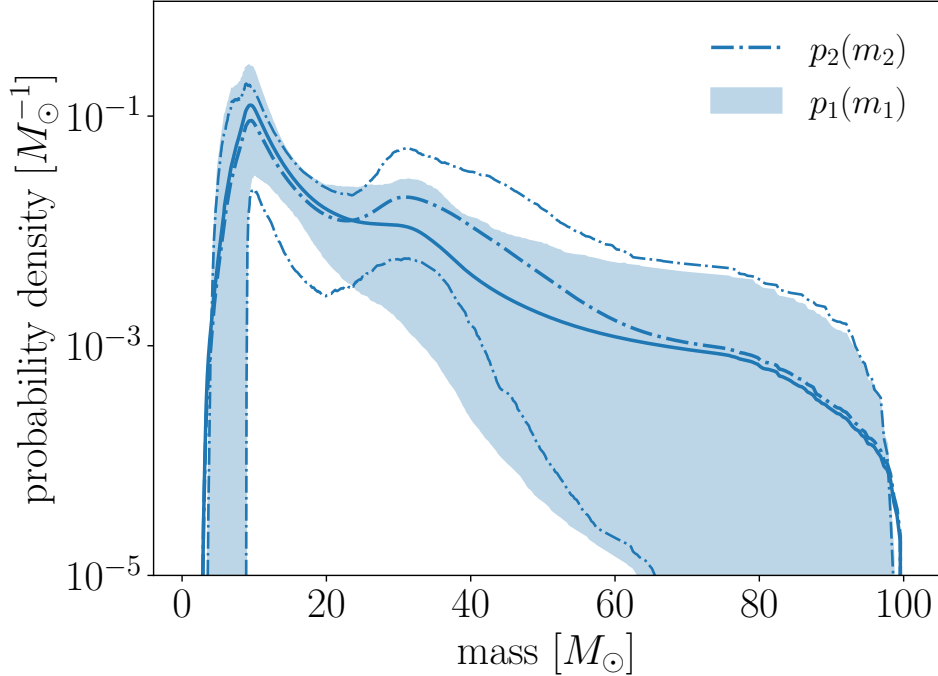


Figure 9. Underlying distributions (i.e. before a pairing function is applied) of the primary (*shaded band*) and secondary (*dot-dashed lines*) masses under the most general form of the base model. Despite fitting all parameters separately between the two distributions, they appear consistent with one another. However, both are relatively poorly constrained. Interestingly, the support for a peak in $p_1(m_1)$ lessens in this more generalized model, while the support for a peak in $p_2(m_2)$ remains the same as in PAIRING:GENERIC.

is the fraction of detectable events in a population described by Λ , and $P(\text{det}|m_1, m_2, s_1, s_2, z)$ is the probability that any individual event with parameters m_1, m_2, s_1, s_2 , and z would be detected, averaged over the duration of the experiment.

In practice, the high-dimensional integrals in Eqs. C8 and C9 are approximated via importance sampling (see Essick & Farr 2022; Essick & Fishbach 2021, for a detailed explanation of this process). Given a set of N_j event-level samples drawn from the posterior for the j^{th} event that used a reference prior $p_{\text{ref}}(m_1, m_2, s_1, s_2, z)$, we approximate

$$\frac{p(D_j|\Lambda)}{p_{\text{ref}}(D_j)} \approx \frac{1}{N_j} \sum_k^{N_j} \frac{p(m_1^{(k)}, m_2^{(k)}, s_1^{(k)}, s_2^{(k)}, z^{(k)}|\Lambda)}{p_{\text{ref}}(m_1^{(k)}, m_2^{(k)}, s_1^{(k)}, s_2^{(k)}, z^{(k)})} \quad (\text{C10})$$

where $p_{\text{ref}}(D_j)$, the marginal likelihood for D_j under the reference prior, does not depend on Λ and therefore need not be included when determining the population fit. Similarly, by simulating a large set of M signals drawn from an injected population p_{draw} , we can approximate Eq. C9 with a sum over the subset of m detected signals

$$\mathcal{E}(\Lambda) \approx \frac{1}{M} \sum_k^m \frac{p(m_1^{(k)}, m_2^{(k)}, s_1^{(k)}, s_2^{(k)}, z^{(k)}|\Lambda)}{p_{\text{draw}}(m_1^{(k)}, m_2^{(k)}, s_1^{(k)}, s_2^{(k)}, z^{(k)})} \quad (\text{C11})$$

We obtain the detectable set of m signals by injecting waveforms of these signals into the measured detector strain and running the search pipelines (Usman et al. 2016; Aubin et al. 2021; Drago et al. 2021; Cannon et al. 2021) used by the LVK to detect events to obtain a false alarm rate (FAR) for each injected signal. This process was performed by the LVK for its population analysis (Abbott et al. 2023a) and we use the resulting publicly-released data product in this work (Collaboration 2021). We then consider an event detected if it has a FAR of less than 1/year in at least one pipeline, and apply this threshold both to injected signals and the real GW events in GWTC-3.

We sample from the posterior distribution in Eq. C7 using the approximations in Eqs. C10 and C11 to determine the shape of the mass distribution using `gwpopulation` (Talbot et al. 2019) with the nested sampling algorithm `dynesty`

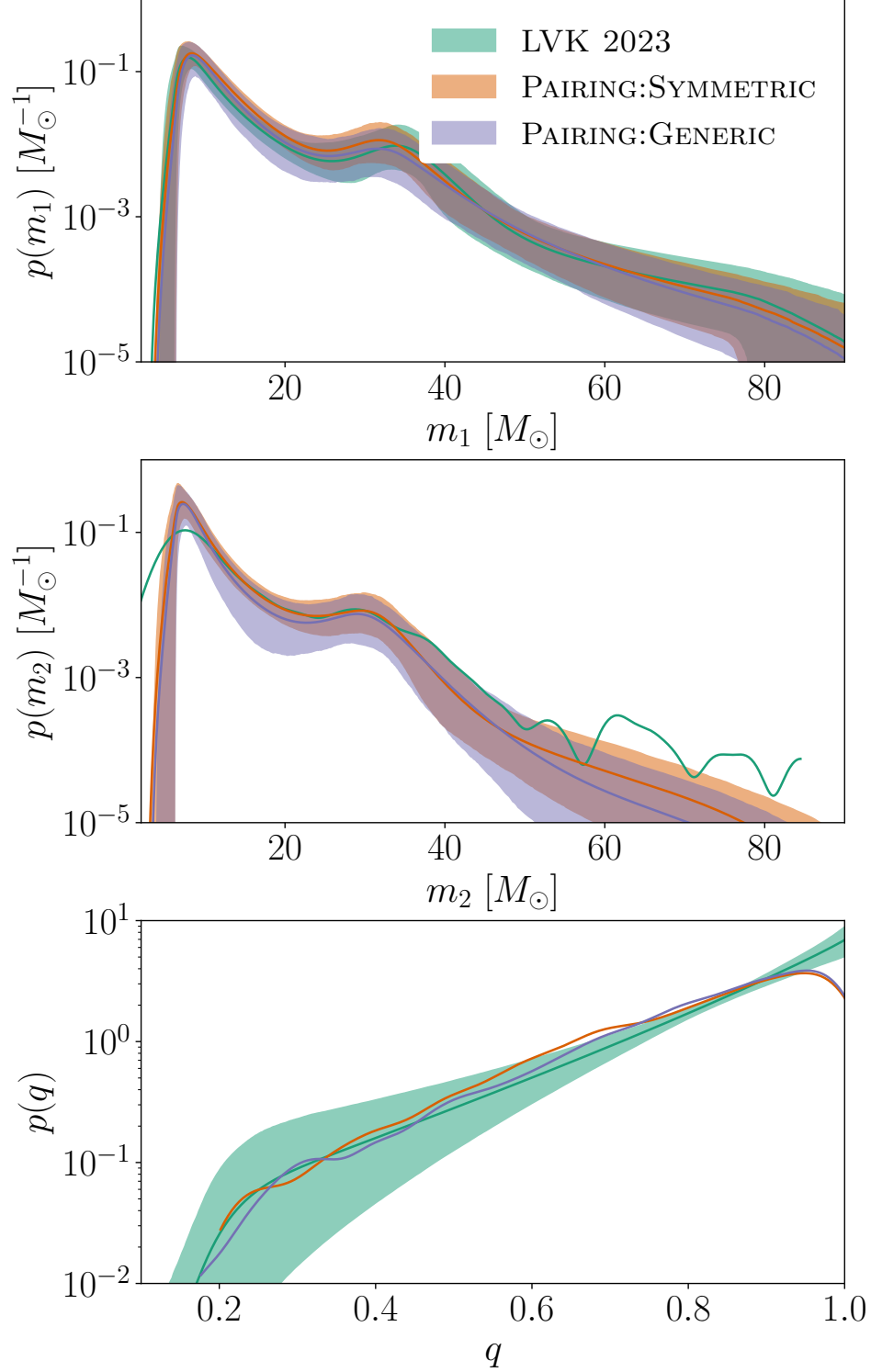


Figure 10. Marginal PPDs of primary mass (*top*), secondary mass (*middle*) and mass ratio (*bottom*) for CONDITIONED-Q (*green*), PAIRING:SYMMETRIC (*orange*) and PAIRING:GENERIC (*purple*). Solid lines are the mean value and shaded regions represent the 90% credible interval. These are obtained by integrating the 2D PPDs shown in Figure 2 along each dimension in turn. Since the CONDITIONED-Q model is parameterized in terms of m_1 and q , we reconstruct its marginal m_2 distribution by sampling from the joint distribution and creating a kernel density estimate, causing some artificial “wiggles” in these plots. The same is true for the marginal q distributions of the pairing function models. Despite the 2D PPDs appearing different between CONDITIONED-Q and the other two models, the marginal PPDs all appear similar. This is because features in the primary mass distribution induce features in the marginal secondary mass distribution if equal-mass binaries are preferred. Therefore, marginal PPDs are not sensitive to the features in the 2D mass distribution in which we are interested.

| Parameter | Description | Prior | | |
|--------------|--|-----------------------------------|---------------------------|-------------------|
| | | Base model | PAIRING:GENERIC | PAIRING:SYMMETRIC |
| β_q | Spectral index for the power law of the pairing function. | U(-4, 12) | | - |
| β | Spectral index for the power law of the mass ratio distribution. | - | | U(-4, 12) |
| α_1 | Spectral index for the power law of the primary mass distribution | U(-4, 12) | | |
| α_2 | Spectral index for the power law of the secondary mass distribution | U(-4, 12) | $\alpha_2 = \alpha_1$ | - |
| $m_{\min,1}$ | Minimum mass of the primary mass distribution. | U($2 M_\odot$, $10 M_\odot$) | | |
| $m_{\min,2}$ | Minimum mass of the secondary mass distribution. | U($2 M_\odot$, $10 M_\odot$) | $m_{\min,2} = m_{\min,1}$ | - |
| $m_{\max,1}$ | Maximum mass of the primary mass distribution. | U($30 M_\odot$, $100 M_\odot$) | | |
| $m_{\max,2}$ | Maximum mass of the secondary mass distribution. | U($30 M_\odot$, $100 M_\odot$) | $m_{\max,2} = m_{\max,1}$ | - |
| δ_1 | Range of tapering at the low end of the primary mass distribution. | U($0 M_\odot$, $10 M_\odot$) | | |
| δ_2 | Range of tapering at the low end of the secondary mass distribution. | U($0 M_\odot$, $10 M_\odot$) | $\delta_2 = \delta_1$ | - |
| λ_1 | Fraction of systems with primary mass in the Gaussian component. | U(0, 1) | | |
| λ_2 | Fraction of systems with secondary mass in the Gaussian component. | U(0,1) | $\lambda_2 = \lambda_1$ | - |
| μ_1 | Mean of the Gaussian component in the primary mass distribution. | U($20 M_\odot$, $50 M_\odot$) | | |
| μ_2 | Mean of the Gaussian component in the secondary mass distribution. | U($20 M_\odot$, $50 M_\odot$) | $\mu_2 = \mu_1$ | - |
| σ_1 | Width of the Gaussian component in the primary mass distribution. | U($1 M_\odot$, $10 M_\odot$) | | |
| σ_2 | Width of the Gaussian component in the secondary mass distribution. | U($1 M_\odot$, $10 M_\odot$) | $\sigma_2 = \sigma_1$ | - |

Table 1. Hyperparameters of our mass model and hyperpriors corresponding to specific model variations. For comparison, we also show the hyperpriors for the CONDITIONED-Q model. We denote the uniform distribution between x and y as $U(x, y)$, list specific values that are fixed in some priors, and denote when hyperparameters are irrelevant to a specific nested model with “-”.

(Speagle 2020). Furthermore, where needed, we estimate Bayes factors via Savage-Dickey Density Ratios (Dickey & Lientz 1970; Wagenmakers et al. 2010) using the hyperposteriors and the hyperpriors described in Section B.1.

REFERENCES

- 1998, Two of a Kind, ABC.
<http://web.archive.org/web/20000510080526/http://www.mary-kateandashley.com/>
- Aasi, J., Abbott, B. P., Abbott, R., et al. 2015, Classical and Quantum Gravity, 32, 074001, doi: 10.1088/0264-9381/32/7/074001
- Abbott, B. P., Abbott, R., Abbott, T. D., et al. 2019, Physical Review X, 9, 031040, doi: 10.1103/PhysRevX.9.031040
- Abbott, R., Abbott, T. D., Acernese, F., et al. 2021a, <https://ui.adsabs.harvard.edu/abs/2021arXiv211103606T>

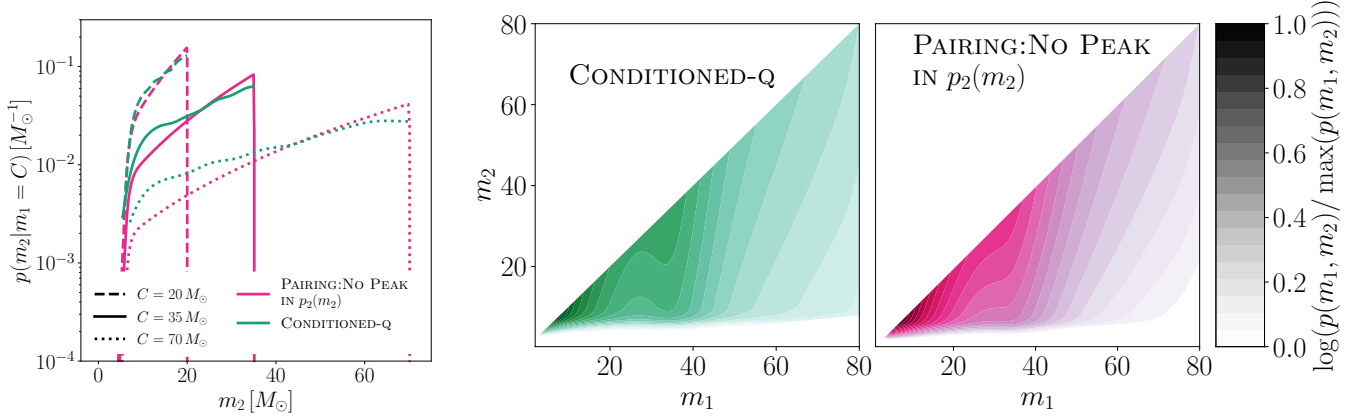


Figure 11. Two-dimensional (*right*) and conditional m_2 (*left*) PPDs for the CONDITIONED-Q and PAIRING:NO PEAK IN $p_2(m_2)$ models.

- Abbott, R., Abbott, T. D., Abraham, S., et al. 2021b, *The Astrophysical Journal Letters*, 913, L7, doi: [10.3847/2041-8213/abe949](https://doi.org/10.3847/2041-8213/abe949)
- Abbott, R., Abbott, T. D., Acernese, F., et al. 2023a, *Physical Review X*, 13, 011048, doi: [10.1103/PhysRevX.13.011048](https://doi.org/10.1103/PhysRevX.13.011048)
- Abbott, R., Abe, H., Acernese, F., et al. 2023b, *The Astrophysical Journal*, 949, 76, doi: [10.3847/1538-4357/ac74bb](https://doi.org/10.3847/1538-4357/ac74bb)
- . 2023c, *The Astrophysical Journal Supplement Series*, 267, 29, doi: [10.3847/1538-4365/acdc9f](https://doi.org/10.3847/1538-4365/acdc9f)
- Acernese, F., Agathos, M., Agatsuma, K., et al. 2014, *Classical and Quantum Gravity*, 32, 024001, doi: [10.1088/0264-9381/32/2/024001](https://doi.org/10.1088/0264-9381/32/2/024001)
- Akutsu, T., Ando, M., Arai, K., et al. 2021, *Progress of Theoretical and Experimental Physics*, 2021, 05A101, doi: [10.1093/ptep/ptaa125](https://doi.org/10.1093/ptep/ptaa125)
- Ashton, G., Hübner, M., Lasky, P. D., et al. 2019, 241, 27, doi: [10.3847/1538-4365/ab06fc](https://doi.org/10.3847/1538-4365/ab06fc)
- Aubin, F., Brighenti, F., Chierici, R., et al. 2021, *Classical and Quantum Gravity*, 38, 095004, doi: [10.1088/1361-6382/abe913](https://doi.org/10.1088/1361-6382/abe913)
- Baxter, E. J., Croon, D., McDermott, S. D., & Sakstein, J. 2021, *The Astrophysical Journal*, 916, L16, doi: [10.3847/2041-8213/ac11fc](https://doi.org/10.3847/2041-8213/ac11fc)
- Bayarri, M. J., & Castellanos, M. E. 2007, *Statistical Science*, 22, 322, doi: [10.1214/07-STS235](https://doi.org/10.1214/07-STS235)
- Broekgaarden, F. S., Stevenson, S., & Thrane, E. 2022, *The Astrophysical Journal*, 938, 45, doi: [10.3847/1538-4357/ac8879](https://doi.org/10.3847/1538-4357/ac8879)
- Callister, T. A., & Farr, W. M. 2023, *A Parameter-Free Tour of the Binary Black Hole Population*, arXiv, doi: [10.48550/arXiv.2302.07289](https://doi.org/10.48550/arXiv.2302.07289)
- Callister, T. A., Haster, C.-J., Ng, K. K. Y., Vitale, S., & Farr, W. M. 2021, *The Astrophysical Journal Letters*, 922, L5, doi: [10.3847/2041-8213/ac2ccc](https://doi.org/10.3847/2041-8213/ac2ccc)
- Cannon, K., Caudill, S., Chan, C., et al. 2021, *SoftwareX*, 14, 100680, doi: [10.1016/j.softx.2021.100680](https://doi.org/10.1016/j.softx.2021.100680)
- Chernoff, D. F., & Finn, L. S. 1993, *The Astrophysical Journal*, 411, L5, doi: [10.1086/186898](https://doi.org/10.1086/186898)
- Collaboration, L. S. C. a. V. C. a. K. 2021, *GWTC-3: Compact Binary Coalescences Observed by LIGO and Virgo During the Second Part of the Third Observing Run — O3 search sensitivity estimates*, Zenodo, doi: [10.5281/zenodo.5546676](https://doi.org/10.5281/zenodo.5546676)
- Dickey, J. M., & Lientz, B. P. 1970, *The Annals of Mathematical Statistics*, 41, 214. <https://www.mendeley.com/catalogue/ff8e9252-ad6c-37f5-9e8f-8a48de0e2a06/>
- Doctor, Z., Wysocki, D., O’Shaughnessy, R., Holz, D. E., & Farr, B. 2020, *The Astrophysical Journal*, 893, 35, doi: [10.3847/1538-4357/ab7fac](https://doi.org/10.3847/1538-4357/ab7fac)
- Drago, M., Klimentko, S., Lazzaro, C., et al. 2021, *SoftwareX*, 14, 100678, doi: [10.1016/j.softx.2021.100678](https://doi.org/10.1016/j.softx.2021.100678)
- Edelman, B., Doctor, Z., Godfrey, J., & Farr, B. 2022a, *The Astrophysical Journal*, 924, 101, doi: [10.3847/1538-4357/ac3667](https://doi.org/10.3847/1538-4357/ac3667)
- Edelman, B., Farr, B., & Doctor, Z. 2022b, *Cover Your Basis: Comprehensive Data-Driven Characterization of the Binary Black Hole Population*, Tech. rep. <https://ui.adsabs.harvard.edu/abs/2022arXiv221012834E>
- Essick, R., & Farr, W. 2022, *Precision Requirements for Monte Carlo Sums within Hierarchical Bayesian Inference*, Tech. rep. <https://ui.adsabs.harvard.edu/abs/2022arXiv220400461E>
- Essick, R., & Fishbach, M. 2021, *On Estimating Rates from Monte-Carlo Integrals over Injection Sets*. <https://dcc.ligo.org/T2000100>

- Ezquiaga, J. M., & Holz, D. E. 2021, *The Astrophysical Journal*, 909, L23, doi: [10.3847/2041-8213/abe638](https://doi.org/10.3847/2041-8213/abe638)
- . 2022, *Physical Review Letters*, 129, 061102, doi: [10.1103/PhysRevLett.129.061102](https://doi.org/10.1103/PhysRevLett.129.061102)
- Farag, E., Renzo, M., Farmer, R., Chidester, M. T., & Timmes, F. X. 2022, *The Astrophysical Journal*, 937, 112, doi: [10.3847/1538-4357/ac8b83](https://doi.org/10.3847/1538-4357/ac8b83)
- Farah, A., Fishbach, M., Essick, R., Holz, D. E., & Galadage, S. 2022, *The Astrophysical Journal*, 931, 108, doi: [10.3847/1538-4357/ac5f03](https://doi.org/10.3847/1538-4357/ac5f03)
- Farah, A. M., Edelman, B., Zevin, M., et al. 2023, Things that might go bump in the night: Assessing structure in the binary black hole mass spectrum, Tech. rep., doi: [10.48550/arXiv.2301.00834](https://doi.org/10.48550/arXiv.2301.00834)
- Farmer, R., Renzo, M., de Mink, S., Fishbach, M., & Justham, S. 2020, *The Astrophysical Journal*, 902, L36, doi: [10.3847/2041-8213/abbadd](https://doi.org/10.3847/2041-8213/abbadd)
- Farmer, R., Renzo, M., de Mink, S. E., Marchant, P., & Justham, S. 2019, *The Astrophysical Journal*, 887, 53, doi: [10.3847/1538-4357/ab518b](https://doi.org/10.3847/1538-4357/ab518b)
- Farr, W. M., Fishbach, M., Ye, J., & Holz, D. E. 2019, *The Astrophysical Journal*, 883, L42, doi: [10.3847/2041-8213/ab4284](https://doi.org/10.3847/2041-8213/ab4284)
- Fishbach, M., Farr, W. M., & Holz, D. E. 2020, *The Astrophysical Journal*, 891, L31, doi: [10.3847/2041-8213/ab77c9](https://doi.org/10.3847/2041-8213/ab77c9)
- Fishbach, M., & Holz, D. E. 2017a, *The Astrophysical Journal*, 851, L25, doi: [10.3847/2041-8213/aa9bf6](https://doi.org/10.3847/2041-8213/aa9bf6)
- . 2017b, arXiv:1709.08584 [astro-ph, physics:gr-qc]. <http://arxiv.org/abs/1709.08584>
- . 2020, *The Astrophysical Journal*, 891, L27, doi: [10.3847/2041-8213/ab7247](https://doi.org/10.3847/2041-8213/ab7247)
- Fishbach, M., Holz, D. E., & Farr, W. M. 2018, *The Astrophysical Journal*, 863, L41, doi: [10.3847/2041-8213/aad800](https://doi.org/10.3847/2041-8213/aad800)
- Foreman-Mackey, D. 2016, *Journal of Open Source Software*, 1, 24, doi: [10.21105/joss.00024](https://doi.org/10.21105/joss.00024)
- Gelman, A. 2006, *Bayesian Analysis*, 1, 515, doi: [10.1214/06-BA117A](https://doi.org/10.1214/06-BA117A)
- Godfrey, J., Edelman, B., & Farr, B. 2023, Cosmic Cousins: Identification of a Subpopulation of Binary Black Holes Consistent with Isolated Binary Evolution, doi: [10.48550/arXiv.2304.01288](https://doi.org/10.48550/arXiv.2304.01288)
- Grudić, M. Y., Offner, S. S. R., Guszejnov, D., Faucher-Giguère, C.-A., & Hopkins, P. F. 2023, Does God play dice with star clusters?, arXiv, doi: [10.48550/arXiv.2307.00052](https://doi.org/10.48550/arXiv.2307.00052)
- Heger, A., & Woosley, S. E. 2002, *The Astrophysical Journal*, 567, 532, doi: [10.1086/338487](https://doi.org/10.1086/338487)
- Hu, R.-C., Zhu, J.-P., Qin, Y., et al. 2022, *The Astrophysical Journal*, 928, 163, doi: [10.3847/1538-4357/ac573f](https://doi.org/10.3847/1538-4357/ac573f)
- Kiendrebeogo, R. W., Farah, A. M., Foley, E. M., et al. 2023, Updated observing scenarios and multi-messenger implications for the International Gravitational-wave Network's O4 and O5, arXiv, doi: [10.48550/arXiv.2306.09234](https://doi.org/10.48550/arXiv.2306.09234)
- Kovetz, E. D., Cholis, I., Breyse, P. C., & Kamionkowski, M. 2017, *Physical Review D*, 95, 103010, doi: [10.1103/PhysRevD.95.103010](https://doi.org/10.1103/PhysRevD.95.103010)
- Laplace, E., Justham, S., Renzo, M., et al. 2021, *Astronomy and Astrophysics*, 656, A58, doi: [10.1051/0004-6361/202140506](https://doi.org/10.1051/0004-6361/202140506)
- Loredo, T. J. 2004, 735, 195, doi: [10.1063/1.1835214](https://doi.org/10.1063/1.1835214)
- . 2013, Bayesian Astrostatistics: A Backward Look to the Future (eprint: arXiv:1208.3036), doi: [10.1007/978-1-4614-3508-2_2](https://doi.org/10.1007/978-1-4614-3508-2_2)
- Mandel, I., & Farmer, A. 2022, *Physics Reports*, 955, 1, doi: [10.1016/j.physrep.2022.01.003](https://doi.org/10.1016/j.physrep.2022.01.003)
- Mandel, I., Farr, W. M., & Gair, J. R. 2019, *Monthly Notices of the Royal Astronomical Society*, 486, 1086, doi: [10.1093/mnras/stz896](https://doi.org/10.1093/mnras/stz896)
- Mapelli, M. 2020, *Frontiers in Astronomy and Space Sciences*, 7, 38, doi: [10.3389/fspas.2020.00038](https://doi.org/10.3389/fspas.2020.00038)
- Messenger, C., & Read, J. 2012, *Physical Review Letters*, 108, 091101, doi: [10.1103/PhysRevLett.108.091101](https://doi.org/10.1103/PhysRevLett.108.091101)
- Mould, M., Gerosa, D., Broekgaarden, F. S., & Steinle, N. 2022, *Monthly Notices of the Royal Astronomical Society*, 517, 2738, doi: [10.1093/mnras/stac2859](https://doi.org/10.1093/mnras/stac2859)
- Olejak, A., & Belczynski, K. 2021, *The Astrophysical Journal Letters*, 921, L2, doi: [10.3847/2041-8213/ac2f48](https://doi.org/10.3847/2041-8213/ac2f48)
- Ray, A., Magaña Hernandez, I., Mohite, S., Creighton, J., & Kapadia, S. 2023, Non-parametric inference of the population of compact binaries from gravitational wave observations using binned Gaussian processes, Tech. rep., doi: [10.48550/arXiv.2304.08046](https://doi.org/10.48550/arXiv.2304.08046)
- Sadiq, J., Dent, T., & Gieles, M. 2023, Binary vision: The merging black hole binary mass distribution via iterative density estimation, arXiv, doi: [10.48550/arXiv.2307.12092](https://doi.org/10.48550/arXiv.2307.12092)
- Sadiq, J., Dent, T., & Wysocki, D. 2022, *Physical Review D*, 105, 123014, doi: [10.1103/PhysRevD.105.123014](https://doi.org/10.1103/PhysRevD.105.123014)
- Sinharay, S., & Stern, H. S. 2003, *Journal of Statistical Planning and Inference*, 111, 209, doi: [10.1016/S0378-3758\(02\)00303-8](https://doi.org/10.1016/S0378-3758(02)00303-8)
- Speagle, J. S. 2020, *Monthly Notices of the Royal Astronomical Society*, 493, 3132, doi: [10.1093/mnras/staa278](https://doi.org/10.1093/mnras/staa278)

- Stevenson, S., Ohme, F., & Fairhurst, S. 2015, *The Astrophysical Journal*, 810, 58, doi: [10.1088/0004-637X/810/1/58](https://doi.org/10.1088/0004-637X/810/1/58)
- Stevenson, S., Sampson, M., Powell, J., et al. 2019, *The Astrophysical Journal*, 882, 121, doi: [10.3847/1538-4357/ab3981](https://doi.org/10.3847/1538-4357/ab3981)
- Talbot, C., Smith, R., Thrane, E., & Poole, G. B. 2019, *Physical Review D*, 100, 043030, doi: [10.1103/PhysRevD.100.043030](https://doi.org/10.1103/PhysRevD.100.043030)
- Talbot, C., & Thrane, E. 2018, *The Astrophysical Journal*, 856, 173, doi: [10.3847/1538-4357/aab34c](https://doi.org/10.3847/1538-4357/aab34c)
- Taylor, S. R., Gair, J. R., & Mandel, I. 2012, *Physical Review D*, 85, 023535, doi: [10.1103/PhysRevD.85.023535](https://doi.org/10.1103/PhysRevD.85.023535)
- Tiwari, V. 2021, *Classical and Quantum Gravity*, 38, 155007, doi: [10.1088/1361-6382/ac0b54](https://doi.org/10.1088/1361-6382/ac0b54)
- . 2023, What's in a binary black hole's mass parameter?, doi: [10.48550/arXiv.2304.03498](https://doi.org/10.48550/arXiv.2304.03498)
- Usman, S. A., Nitz, A. H., Harry, I. W., et al. 2016, *Classical and Quantum Gravity*, 33, 215004, doi: [10.1088/0264-9381/33/21/215004](https://doi.org/10.1088/0264-9381/33/21/215004)
- Virtanen, P., Gommers, R., Oliphant, T. E., et al. 2020, *Nature Methods*, 17, 261, doi: [10.1038/s41592-019-0686-2](https://doi.org/10.1038/s41592-019-0686-2)
- Wagenmakers, E.-J., Lodewyckx, T., Kuriyal, H., & Grasman, R. 2010, *Cognitive Psychology*, 60, 158, doi: [10.1016/j.cogpsych.2009.12.001](https://doi.org/10.1016/j.cogpsych.2009.12.001)
- Zevin, M., & Bavera, S. S. 2022, *The Astrophysical Journal*, 933, 86, doi: [10.3847/1538-4357/ac6f5d](https://doi.org/10.3847/1538-4357/ac6f5d)
- Zevin, M., Pankow, C., Rodriguez, C. L., et al. 2017, *The Astrophysical Journal*, 846, 82, doi: [10.3847/1538-4357/aa8408](https://doi.org/10.3847/1538-4357/aa8408)